

# An Approach for the Concurrent Homogenization-based Microstructure Type and Topology Optimization Problem

Konstantinos-Iason Ypsilantis<sup>a,\*</sup>, Matthias G.R. Faes<sup>b</sup>, Jan Ivens<sup>c</sup>, Nikos D. Lagaros<sup>d</sup> and David Moens<sup>a,\*\*</sup>

<sup>a</sup>*KU Leuven, Department of Mechanical Engineering, Div. LMSD, Jan De Nayerlaan 5, 2860, Sint-Katelijne-Waver, Belgium*

<sup>b</sup>*TU Dortmund University, Chair for Reliability Engineering, Leonard-Euler-straße 5, 44227 Dortmund, Germany*

<sup>c</sup>*KU Leuven, Department of Materials Engineering, Structural Composites and Alloys, Integrity and Nondestructive Testing, Jan De Nayerlaan 5, 2860, Sint-Katelijne-Waver, Belgium*

<sup>d</sup>*National Technical University of Athens, Department of Structural Engineering, Institute of Structural Analysis & Antiseismic Research, School of Civil Engineering, Heron Polytechniou Str. 9, Zografou Campus, GR-15780Athens, Greece*

---

## ARTICLE INFO

### Keywords:

- Topology optimization
- Homogenization type
- 3D unit cell configuration
- Microstructure type optimization
- Multi-material optimization
- Shape function with penalization technique

## Abstract

This work proposes a methodology for the concurrent homogenization-based optimization of the type and the configuration of the microstructure of the structural domain, based on a list of pre-defined composite microstructures. The candidate microstructures are represented on this list by their homogenized mechanical properties, as predicted by means of the 3D homogenization theory. As such, each candidate property is tied to a specific microstructure -the one it has been derived from- and is conditioned on its topology, *i.e.* the geometric configuration of its unit cell. Similar to the standard discrete multi-material optimization problem (DMOP), in order to identify per element/patch in the structural domain the optimal microstructure from that list, weights are assigned to the candidate homogenized properties, with respect to which the final discrete microstructure type optimization problem (DMTOP) is posed. The topology of the optimal microstructure is determined by the volume constraint(s) imposed on one or more of its material components in the homogenization-based topology optimization problem (HTOP). The aim of this work is to combine the DMTOP with the HTOP in a unique mathematical framework in order to determine a unique microstructure type per element/patch in the structural domain, concurrently optimized in its topology. The proposed methodology is built step-by-step through the introduction of four microstructure types of two distinct constituent materials. Upon these auxiliary microstructures, the generalized concurrent homogenization-based topology and discrete microstructure type optimization problem (HTDMOP) is formulated for compliance minimization of the structure. Further, it is illustrated how the DMOP can be perceived as a DMTOP, and hence be combined in a similar fashion with the HTOP for the concurrent homogenization-based topology and material optimization (HTMO) of the structural domain. The paper concludes with demonstrating the developed methodology on the benchmark academic case study of the 3D Messerschmitt-Bölkow-Blohm (MBB) beam for the case where the auxiliary microstructures are considered as candidates for the domain.

---

## 1. Introduction

The employment of composite materials has exponentially expanded over the last decades. Especially in aerospace and automotive applications, where a combination of high material strength and low structural weight is required, it has set the scene for many (r)evolutions in current engineering practice (Rana & Figueiro (2006)). Exploiting the high specific properties of the material constitutes the core of new design paradigms with composites, making composite solutions extremely attractive over conventional homogeneous materials and ideal candidates for numerous types of optimization problems. However, the application of high-end numerical design optimization methods such as topology

---

\*Corresponding author: [konstantinos.ypsilantis@kuleuven.be](mailto:konstantinos.ypsilantis@kuleuven.be)

\*\*Principal corresponding author: [david.moens@kuleuven.be](mailto:david.moens@kuleuven.be)

optimization (TO) remains an open question, despite the large potential for further exploiting the specific advantages of composite materials.

In structural design, optimization is the iterative procedure of constantly adjusting the structure's design variables in order to meet a number of initially selected criteria, while satisfying at the same time a set of imposed constraints. The selection of the design variables varies based on the design criteria to be met, whether the latter involve minimizing the structural weight, the manufacturing and/or the maintenance cost, etc. The objective of TO is to reduce the structural mass by removing as much material as required while ending up with an optimized structure still capable of safely withstanding the imposed loads. The "how" the material can be effectively redistributed throughout the design domain under these constraints constitutes the objective of TO. To achieve this, TO solution approaches search for the density field that optimizes a certain physical quantity (*e.g.* compliance, structural mass, etc.), called the *objective function* of the topology optimization problem (TOP). The objective function to be optimized is subjected to a certain set of constraints that the candidate designs should satisfy at each iteration of the TO solution procedure. In case homogeneous, isotropic materials are considered in the TOP, common practice is to employ the state-of-the-art SIMP method (Bendsøe (1989), Zhou & Rozvany (1991)). The concept of the method is based on the introduction of an artificial, spatial and dimensionless design variable, called the *relative density*. The relative density is defined as the ratio of the existing density of the material at a fixed point in the domain over the density of the same solid material, as such it is bounded within the  $[0, 1]$  range. A relative density value equal to one assigns material within the domain, while values equal to zero constitute the void regions of the domain. A more comprehensive elaboration of the method is found in the textbooks by Rozvany & Olhoff (2001), Bendsøe & Sigmund (2004) and Christensen & Klarbring (2009). Regarding the numerical implementation of the method, in line with the 99-line MATLAB code published in Sigmund (2001), educational papers providing compact and efficient MATLAB codes have significantly contributed to a better comprehension and further development of the field (see *e.g.* Andreassen et al. (2011); Liu & Tovar (2014); Ferrari & Sigmund (2020)). An up to date complete list of open- source SIMP based TO algorithms is summarized in the recent work of Kumar & Suresh (2021).

One of the earliest methods in the field of TO is the homogenization method (Bendsøe & Kikuchi (1988)); via the homogenization method linking between the two scales is accomplished, where in the first step the macroscopic properties of the periodical repetitive microstructure are derived under micromechanical considerations, and in the second step the calculated equivalent properties are considered for the macrostructural analysis. The theory of the method is found in Bensoussan et al. (1978), Hassani & Hinton (1998c), Bendsøe & Sigmund (2004) and a more in detail insight is provided in the textbook of Allaire (2002), while several applications of the theory are found in Hassani & Hinton (1998a,b); Monteiro (2017); Allaire et al. (2019); Wu et al. (2019); Groen et al. (2020).

Regarding the continuous multi-scale topology optimization framework, two separate cases are distinguished: in the first case, the macrostructural level is represented by the periodical repetition of only *one type of microstructure* in the span of the design domain. In this case, the objective is to find the optimal material distribution in the microstructural level for the stress field imposed by the macrostructure. Some early work in this field can be seen by [Fujii et al. \(2001\)](#) and [Wang et al. \(2016\)](#), while in the same framework lies the work of [Liu et al. \(2008\)](#), where the authors employed the Porous Anisotropic Material with Penalty (RAMP) method for the concurrent but independent optimization of the microstructural and the macrostructural topology of the design domain. Regarding the second case, each region of the macrostructure is represented by a *different type of periodically repeating microstructure*. The objective of this TOP is to find the optimal material distribution of each microstructure and concurrently optimize the layout of the macrostructure. In that context, the notable work by [Rodrigues et al. \(2002\)](#) introduced the “separation of scales” concept (or hierarchical optimization), optimizing concurrently the material distribution as well as the local material properties of the elements. Implementing the “separation of scales” concept, [Yan et al. \(2014\)](#) proposed a two-scale topology optimization algorithm by employing the bi-directional evolutionary structural optimization (BESO) ([Xia et al. \(2018\)](#)) method to concurrently update the macro and microstructures of the domain. Similarly, [Chen et al. \(2017\)](#) proposed a concurrent topology optimization approach for finding the optimum topologies of the macrostructures and their corresponding lattice microstructures while imposing the manufacturability constraints that come with the 3D printing process. [Da et al. \(2017\)](#) proposed a multi-phase methodology for concurrent topology optimization of composite structures when the microstructure of the element consists of more than three material phases. [Li et al. \(2018\)](#) proposed the multi-patch microstructures concept for cellular structures, where the macro-structure is featured with the configuration of non-uniformly distributed patches, with each patch consisting of a number of identical material microstructures. In a similar framework, the authors in [Pizzolato et al. \(2019\)](#) proposed a method for the concurrent optimization of the material subdomains’ macro-scale layout and their corresponding microstructures, employing the multi-material level-set method ([Wang et al. \(2015\)](#)) to identify the subdomains and a density approach to represent their microstructures. Following a different approach, a multi-scale finite element method was presented in [Lazarov \(2013\)](#), [Alexandersen & Lazarov \(2015\)](#) and a microstructure projection method in [Pantz & Trabelsi \(2008, 2010\)](#). Finally, 2D and 3D numerical implementations of the concurrent topology optimization for multiscale composite structures, written in MATLAB, are found in the recent work of [Gao et al. \(2019\)](#).

The methodology proposed in this work is motivated by the field of discrete material optimization (DMO) ([Stegmann & Lund \(2005\)](#)), which identifies from a list of pre-defined candidate materials the most suitable one for the structural domain. The candidate materials are represented in the list by their constant mechanical and/or thermophysical properties, and per element ( $e$ ) and/or patch ( $p$ ) in the domain are assigned a specific weight,  $w_{e/p, i} \in [0, 1]$ , with  $i = 1 : n_c$  and  $n_c$  the total number of candidate materials. By that means, the property within

each element/patch is expressed as the weighted sum of the properties of the candidate materials. The scope of the material optimization problem (MOP) is to optimize the objective function with respect to these weights and identify per each element/patch in the domain the most optimal from the list, *i.e.* these weights constitute the design variables of the MOP. Material optimization has been widely used in different applications of laminated composite structures for optimizing the fiber orientation of the uni-directional (UD) laminae from a list of pre-defined candidate ones. In this case, each candidate fiber orientation is indirectly represented in the list by the effective (or off-axis) properties of the corresponding UD lamina.

A less computationally expensive technique compared to DMO when considering  $n_c = 2^k$ , with  $k \in \mathbb{N}^+$ , number of candidate materials, has been introduced in Bruyneel (2011) and Bruyneel et al. (2011), where as weights for the candidate materials are employed the shape functions of the  $2^k$ -noded quadrangular finite element (FE). According to this method, labelled as shape function with penalization (SFP), each candidate material is attached to a specific node on the  $2^k$ -noded quadrangular FE and the optimal nodal location amongst them is requested, *i.e.* the natural coordinate system of the quadrangular FE constitutes the design variables of the MOP. Thus, for a number of  $n_c = 2^k$  candidate materials,  $k = \log_2(n_c)$  design variables are required to determine the optimal one amongst them, reducing that way substantially the dimension of the resulting MOP. As an extension of the SFP technique, allowing the interpolation between  $n_c = [2^{k-1} + 1, 2^k]$  material phases, where  $k = \lceil \log_2(n_c) \rceil$  and  $n_c$  the assumed number of candidate material phases, the bi-value coding parameterization method (BCP) has been proposed in Gao et al. (2012), removing the constraint that the number of candidate material phases should be of integer powers of base 2. The computational advantage of both methods, due to the substantial reduction in the number of design variables has made them preferable to various material optimization problems.

The scope of this work is to propose a methodology for the concurrent optimization of the type, the material components and the topology of the composite microstructure of the structural domain based on a list of pre-defined composite microstructures. To this end, three structural optimization problems are deployed, that of: **(1)** the homogenization-based topology optimization (HTOP), **(2)** the discrete microstructure type optimization (DMTOP), and **(3)** the discrete multi-material optimization (DMOP). The idea is as follows: A catalogue of candidate microstructures considered for the structural domain is provided. The candidate microstructures are represented in this catalogue by their homogenized properties, whether these are their mechanical and/or thermophysical properties. In the present work, however, the homogenization process is carried out only for the mechanical properties of the composite microstructures. The homogenized properties derived from each candidate microstructure are conditioned on its topology, as it is determined by the fraction of the material components within its unit cell configuration. The objective is to optimize the type of the composite microstructure of the structural domain, in accordance with the microstructures listed in the catalogue, and its topology, in accordance with the global volume constraints imposed on one or more of its material components.

Optimizing with respect to the type of the composite microstructure forms the objective of the DMTOP, while optimizing with respect to its topology, under the imposition of global volume constraints, forms the objective of the HTOP. By that means, two types of design variables are distinguished for the resulting optimization problem: **(1)** one that identifies the optimal microstructure type from the given catalogue, and **(2)** one that determines its optimal topology (or corresponding unit cell configuration). Regarding the first type of design variables, and purely due to its computational efficiency, the SFP technique is preferred in this work for interpolating the homogenized properties within the structural domain, thereby introducing the constraint that the number of candidate microstructures should be given in integer powers of base 2. Regarding the second type of design variables, the volume fractions of the candidate microstructures' material components are selected instead of their geometric features, so as to facilitate the formulation of the HTOP.

The developed methodology is constrained to composite microstructures of two material components. Nevertheless, it is illustrated that this limitation can be circumvented by simply listing on the same catalogue microstructures of the same type but of different material components. By that means, under the umbrella of the HTOP, the DMTOP can either be replaced or coexist with the DMOP, while maintaining the same mathematical formulation for the methodology. The overall objective of the methodology is captured in [Figure 1](#) for the case where  $2^k$  two-component microstructure types are considered for each element ( $e$ ) in the structural domain.

To the author's knowledge, bringing together the three aforementioned structural optimization problems under a unique mathematical framework is a topic yet to be explored in the literature.

## 2. Problem statement and structure of the paper

To provide an in-depth insight of the build-out process and the implementation modus of the methodology, it is built step-by-step through a made-up case study; specifically, in the case where a catalogue of four candidate composite microstructure types is considered for the structural domain. The four microstructure types are composed of the same two materials, denoted as *material*<sub>1</sub> and *material*<sub>2</sub>, respectively. The goal is to determine per element ( $e$ ) in the structural domain a unique microstructure out of the four, concurrently optimized in its topology, *i.e.* the fraction of the *material*<sub>1</sub> and *material*<sub>2</sub> components explicitly defining its unit cell configuration. Both the type and the topology of the microstructure predicted per element in the domain depend on the formulation of the volume constraint in the HTOP; that is, on which of the two material components the constraint is to be imposed as well as the fraction of it to be retained in the final domain. To this end, and to proceed further with the development of the methodology, the (arbitrary) assumption is made that the volume constraint is imposed on the *material*<sub>1</sub> component. However, by alternating the properties between the two materials, the volume constraint could as well be imposed on *material*<sub>2</sub>. On the basis of this assumption, the proper design variables are sought for the HTOP in order to efficiently describe the *material*<sub>1</sub> volume

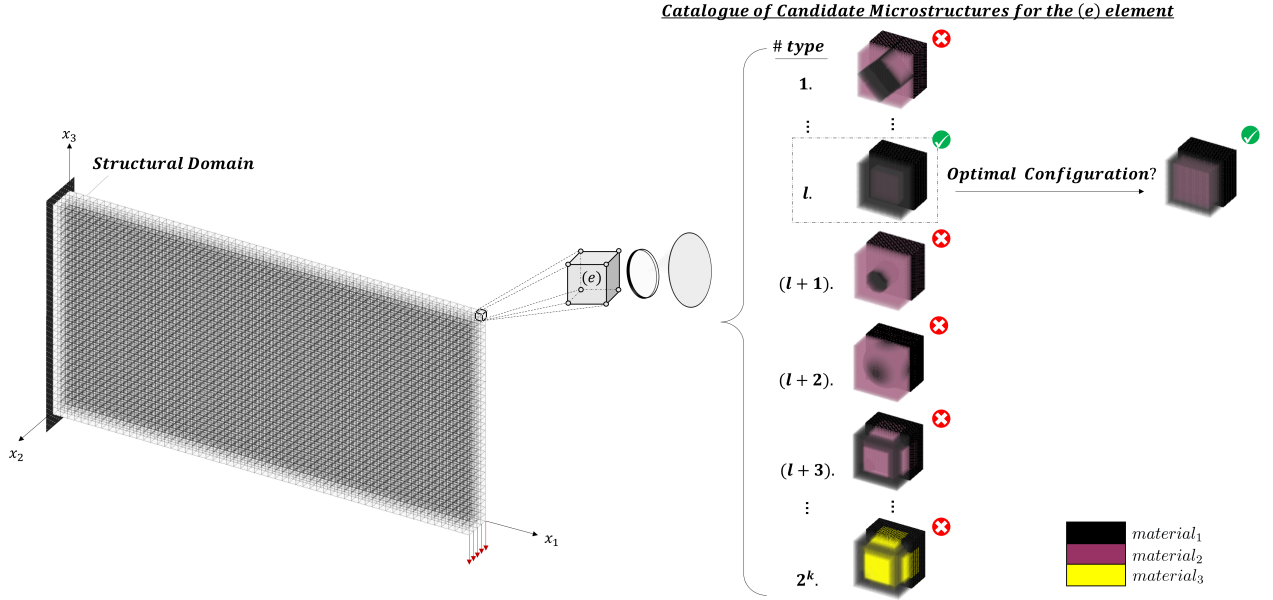


**Figure 1:** The objective of the proposed methodology is to identify from a list of  $2^k$  candidate microstructures considered for the  $(e)$  element in the domain the most optimal one, concurrently optimized in its configuration.

distribution within the structural domain. In terms of computational cost, this translates to identifying amongst the possible types of design variables that can be considered for the HTOP, the ones posing it in its most computationally advantageous yet simplest format. As such, the homogenized properties representing the four candidate microstructure types in the catalogue are expressed in terms of the design variables determined for the HTOP. As a next step, the SFP technique is employed for interpolating the homogenized properties within the structural domain. The mathematical formulation of the concurrent homogenization-based topology and discrete microstructure type optimization problem (HTDMOP) derived from the specific case study is generalized for the case of  $2^k$  candidate microstructures, where  $k \in \mathbb{N}^+$ .

The remainder of the paper is organized as follows: in (Sec. 3), the four elementary composite microstructures are presented and the parameters defining their geometric configuration are specified. The homogenization process is also presented for homogenizing the mechanical properties of the microstructures' different configurations. For completeness, in (Sec. 4), the state-of-the-art DMO technique is deployed for interpolating the microstructures' homogenized properties within the structural domain. However, no further extent to formulating the corresponding DMO-based HTDMOP is given, due to its higher computational cost compared to the SFP-based HTDMOP. In (Sec. 5), the SFP technique is employed for interpolating the homogenized properties within the structural domain. The corresponding SFP-based HTDMOP is posed for the general case of  $2^k$  candidate microstructures for compliance minimization of the structure, under the assumption that the volume constraint is imposed on the *material*<sub>1</sub> component

of the candidate microstructures. In addition, it is demonstrated that the mathematical formulation derived for the SFP-based HTDMOP can be adopted as is for the concurrent homogenization-based topology, microstructure type and/or multi-material optimization of the structure. In (Sec. 6), the developed methodology is demonstrated on the academic case study of the 3D MBB beam, in the case where the auxiliary microstructures are considered candidates for the domain. The same section also discusses different techniques for forcing the solution to converge to the nearest candidate microstructure (*i.e.* discrete design). Amongst them, emphasis is given to a metric developed for measuring the degree of "non-discreteness" in the final design. The paper concludes in (Sec. 7) section where possible extensions and modifications of the proposed methodology are discussed.

### 3. Description of the candidate composite microstructures and derivation of their homogenized mechanical properties

This section describes the pre-processing stage of the methodology, positioned at the microstructural level. The end goal is to express the homogenized properties of the candidate microstructures as a continuous function of the design variables determined for the HTOP, given the assumption that a global volume constraint is imposed on the *material*<sub>1</sub> component. The steps to reach this goal are set out in this section, which is structured as follows: in (Sec. 3.1) the four auxiliary composite microstructure types are first introduced and the parameters determining their geometric configuration are mathematically defined. (Sec. 3.2) briefly discusses the homogenization process and, in particular, homogenizing the mechanical properties of a non-homogeneous unit cell. In (Sec. 3.3), the homogenization process is carried out for different geometric configurations of the candidate composite microstructures. Following, a regression analysis is performed as to model the variation in the homogenized property with respect to the geometric configuration for each microstructure. With a view to facilitating the formulation of the HTOP, the proper design parameters are sought in order to represent the variation in the geometric configuration in the regression analysis process for all microstructures. These parameters will constitute the design variables for the HTOP.

#### 3.1. Description of the candidate microstructure types

Four microstructure types composed of *material*<sub>1</sub> and *material*<sub>2</sub> are considered: (1) a '*Lattice*' one, with the volume of *material*<sub>1</sub> within the unit cell domain being defined by the radius of the arc  $r_L \in \mathbb{R}^+$ , counting from the edges of the unit cell (see Figure 2<sub>(A)</sub>), (2) a '*Box*' one, where the volume of *material*<sub>2</sub> is defined by the length  $\alpha \in \mathbb{R}^+$  of the inner box located at the center of the unit cell, while the rest of the unit cell domain is occupied by *material*<sub>1</sub> (see Figure 2<sub>(B)</sub>), (3) a '*Cylindrical*' and (4) a '*Spherical*' one, with the radius of the cylinder  $r_C \in \mathbb{R}^+$  across the width of the unit cell and of the sphere  $r_S \in \mathbb{R}^+$ , both located at its center, defining the *material*<sub>2</sub> domain (see Figure 2<sub>(C,D)</sub>).

It is noted that in the '*Lattice*' type, the  $r_L$  geometric parameter defines the *material*<sub>1</sub> domain within the unit cell, while the  $(\alpha, r_C, r_S)$  geometric parameters define the *material*<sub>2</sub> domain of the unit cell.

Without loss of generality, more complex and of more geometric parameters microstructures can be considered instead. However, the ones considered in this work are preferred due to: **(1)** their geometric simplicity (*i.e.* the explicit definition of each unit cell's configuration by its uni-variate geometric parameter in combination with the planar and cubic symmetry they display about their center), and **(2)** the collateral computational advantage that comes with considering uni-variate configurations. It is straightforward to extend the method to unit cells with more intricate parametrizations. This however, falls outside the scope of this paper.

### 3.1.1. Discretization of the unit cells

Each unit cell is discretized to an equal number  $n_v \in \mathbb{N}^+$  of FEs per direction, *voxels*, resulting in a total of  $N_v = n_v^3$  FEs in the unit cell. Numerically this is equivalent to modelling the unit cell as a 3D cubic matrix  $[n_v \times n_v \times n_v]$  containing the indexes "1" or "2", depending on which of the two materials has been assigned to each element of the matrix; that is, matrix elements indexed as "1" are allocated the *material*<sub>1</sub> Lamé engineering constants  $(\lambda_1, \mu_1)$ , and matrix elements indexed as "2" are allocated the *material*<sub>2</sub> Lamé engineering constants,  $(\lambda_2, \mu_2)$ . The case of a  $[40 \times 40 \times 40]$  discretization mesh (*i.e.*  $n_v = 40$ ) for the microstructure types considered is depicted in [Figure 4](#). Here, the gray region constitutes the *material*<sub>1</sub> domain within the unit cell while the pink region the *material*<sub>2</sub> domain.

### 3.1.2. Definition of the microstructures' geometric parameters

To sufficiently define the geometric parameter vector of each microstructure type, three quantities are defined first: its lower and upper bound and its sufficient increment step, a mesh-dependent parameter crucial for avoiding possible repetitions of the same configuration:

**Type 1: 'Lattice'**: As depicted in [Figure 2<sub>\(A\)</sub>](#), the FEs with their center located within the arc of radius  $r_L$ , define the *material*<sub>1</sub> domain. The maximum value of the radius equals to:  $r_{L,max} = \sqrt{2 \cdot 0.5^2} = 0.707$  unit cell units, and for computational stability purposes its minimum value is set equal to  $10^{-9}$  unit cell units.

Intermediate values of the radius correspond to intermediate configurations of the '*Lattice*' microstructure. In that way, the radius of the microstructure is expressed in a vector format, with each element in the vector corresponding to a unique configuration for the microstructure. In order to ensure this one-to-one correspondence between the elements in the vector and different configurations of the microstructure, the sufficient increment step  $\delta_{r_L}$  is introduced between two successive radius values, as illustrated in [Figure 3<sub>\(A\)</sub>](#); that is, radii increments lower than  $\delta_{r_L}$  do not suffice to capture the center of the adjacent FEs forming the next configuration, and will result in *repetition* of the current one. Repetition of the current configuration due to an insufficient increment in the radius results in repetition of the homogenized property.

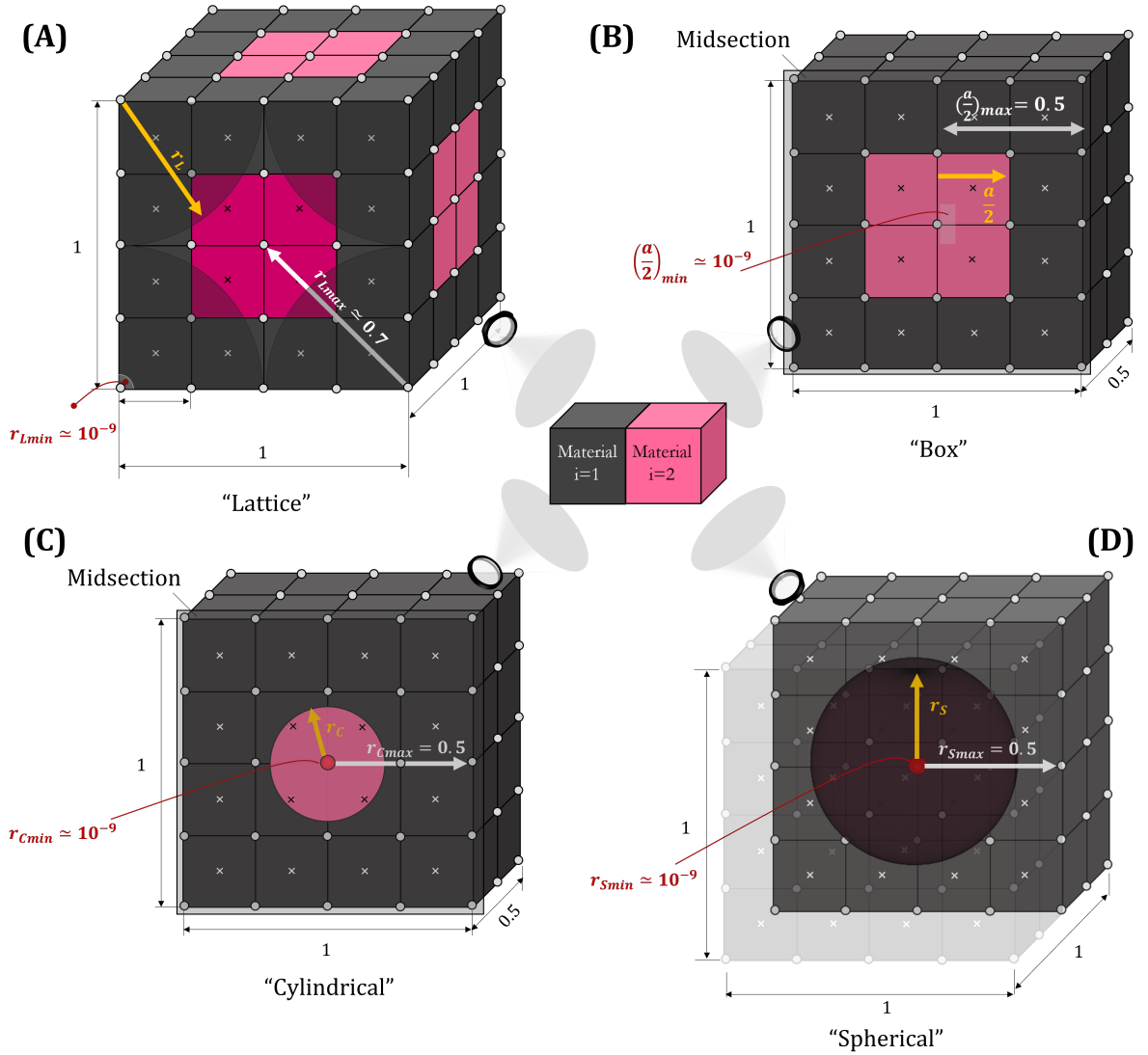


**Figure 2:** Sketch representation of the four microstructure types discretized in a  $[4 \times 4 \times 4]$  mesh: **(A)** FEs within the arc defined by the radius  $r_L$ , constitute the 1<sup>st</sup> material (gray colored region). **(B)** FEs within the inner box, delimited by the  $\frac{a}{2}$  length, constitute the 2<sup>nd</sup> material (pink colored region). **(C)** FEs within the cylinder radius  $r_C$ , constitute the 2<sup>nd</sup> material (pink colored region). **(D)** FEs within the radius of the sphere  $r_S$ , constitute the 2<sup>nd</sup> material (pink colored region).

These data operate as "noise" and are identified as plateau regions in the homogenized property versus the geometric parameter variation graph, diminishing the quality of the regression model to be fitted (discussed in (Sec. 3.3)). As such, the sufficient increment step  $\delta_{r_L}$  defined for the radius is set equal to the diagonal of the FE discretizing its unit cell, *i.e.* the direction along which the radius increases. By that means, the geometric parameter vector for the 'Lattice' microstructure  $\{r_L\}$  is defined as:  $\{r_L\} = [10^{-9} : \delta_{r_L} : 0.707]$ .

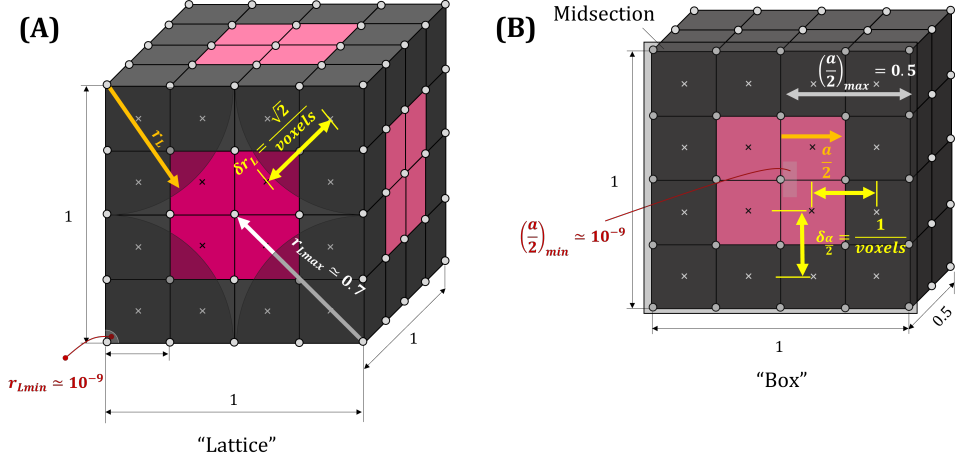


**Figure 3:** Definition of the geometric parameter vector for the  $[4 \times 4 \times 4]$  discretized '*Lattice*' and '*Box*' microstructures: **(A)**  $\{r_L\} = [10^{-9} : \delta_{r_L} : 0.707]$ . **(B)**  $\{\frac{\alpha}{2}\} = [10^{-9} : \delta_{\frac{\alpha}{2}} : 0.5]$ . Increments of the geometric parameter lower than the  $\delta_{r_L}$  and  $\delta_{\frac{\alpha}{2}}$  step, respectively, will result to repetition of the former unit cell configuration. The parameter *voxels* defines the number of FEs discretizing the unit cell per direction, *i.e.* *voxels* = 4 in the figure.

In the same way, to avoid repetition of the same configuration for the rest of the microstructures, a corresponding sufficient step is defined as well. The sufficient steps defined for the '*Lattice*' and '*Box*' microstructures are illustrated in [Figure 3](#).

**Type 2: 'Box':** Regarding the '*Box*' microstructure, the FEs with their center located within the inner box delimited by the  $[-\frac{\alpha}{2}, \frac{\alpha}{2}]$  planes about the unit cell center form the  $2^{nd}$  material. The maximum value of the  $\frac{\alpha}{2}$  parameter is bounded to half the unit cell length, and for computational stability purposes its minimum value is set equal to  $(\frac{\alpha}{2})_{min} = 10^{-9}$  unit cell units. The sufficient step defined for the '*Box*' microstructure equals to the length of the FEs discretizing it. As such, the geometric parameter vector for the '*Box*' microstructure is defined as:  $\{\frac{\alpha}{2}\} = [10^{-9} : \delta_{\frac{\alpha}{2}} : 0.5]$ . The  $\{\frac{\alpha}{2}\}$  vector is illustrated in [Figure3\(B\)](#).

**Types 3, 4: 'Cylindrical' & 'Spherical':** Regarding the '*Cylindrical*' and '*Spherical*' microstructures, the FEs with their center located within the radius of the inner cylinder  $r_C$  and sphere  $r_S$ , respectively, constitute the  $2^{nd}$  material. The maximum value for both radii is reached when the surface of the cylinder/sphere reaches the outer surface of the unit cell. Similar to the '*Lattice*' and the '*Box*' microstructures, the lower bound of  $10^{-9}$  unit cell units is imposed on both radii. As such, the two geometric parameter vectors are defined as:  $\{r_C\} = [10^{-9} : \delta_{r_C} : 0.5]$  and  $\{r_S\} = [10^{-9} : \delta_{r_S} : 0.5]$ , respectively. The sufficient radius increments  $\delta_{r_C}$  and  $\delta_{r_S}$ , equal to the sufficient radius increment of the '*Lattice*' microstructure  $\delta_{r_L}$ .

Table 1: Bounds of the microstructures' geometric parameters (in unit cell units)

<i>'Lattice'</i>	
$r_{L,min}$	$= 10^{-9} \leq \{r_L\} \leq r_{L,max} = 0.707$
<i>'Box'</i>	
$(\frac{\alpha}{2})_{min}$	$= 10^{-9} \leq \{\frac{\alpha}{2}\} \leq (\frac{\alpha}{2})_{max} = 0.5$
<i>'Cylindrical'</i>	
$r_{C,min}$	$= 10^{-9} \leq \{r_C\} \leq r_{C,max} = 0.5$
<i>'Spherical'</i>	
$r_{S,min}$	$= 10^{-9} \leq \{r_S\} \leq r_{S,max} = 0.5$

For notational brevity, the geometric parameters of the microstructures are collected in the unique vector

$$p = [\{r_L\}; \{\frac{\alpha}{2}\}; \{r_C\}; \{r_S\}].$$

### 3.2. Homogenizing the unit cells: Overview of the homogenization theory

Homogenization averages the properties of discrete components that constitute a composite unit cell, and under mechanical considerations (*i.e.* the microstructure is assumed periodically repetitive and the scale ratio  $\epsilon \rightarrow 0$ ) extracts its macroscopic (or equivalent) properties.

In this study, the property to be homogenized is the elasticity tensor of the non-homogeneous unit cells. According to homogenization theory, the equivalent elasticity tensor of the unit cell is calculated by the following volume integral:

$$C_{ijkl}^H = \frac{1}{V_{uc}} \cdot \int_{V_{uc}} C_{pqrs} \cdot (\epsilon_{pq}^{0(ij)} - \epsilon_{pq}^{(ij)}) \cdot (\epsilon_{rs}^{0(kl)} - \epsilon_{rs}^{(kl)}) dV, \quad (1)$$

where  $V_{uc}$  is the volume of the unit cell,  $C_{pqrs}$  is the elasticity tensor varying within the unit cell domain,  $\epsilon_{pq}^{0(ij)}$  denotes the macroscopic strain fields applied on the unit cell (*e.g.* for the 3D case extends to the six components  $\epsilon_{11}^{0(ij)}$ ,  $\epsilon_{22}^{0(ij)}$ ,  $\epsilon_{33}^{0(ij)}$ ,  $\epsilon_{12}^{0(ij)}$ ,  $\epsilon_{23}^{0(ij)}$  and  $\epsilon_{13}^{0(ij)}$ ), and  $\epsilon_{pq}^{(ij)}$  denote the locally varying strain fields. The numerical expression of Eq.(1) is given as:

$$C_{ij}^H = \frac{1}{V_{uc}} \cdot \sum_{e=1}^{N_v} \int_{V_e} (\{\chi_e^{0(i)}\} - \{\chi_e^{(i)}\})^T \cdot [k_e] \cdot (\{\chi_e^{0(j)}\} - \{\chi_e^{(j)}\}) dV, \quad (2)$$

where  $V_{uc}$  is the volume of the unit cell,  $V_e$  the volume of each FE discretizing it,  $i$  and  $j$  the indexes of the strain tensor expressed in Voigt notation (the Voigt notation of the strain field is defined as  $\{\epsilon^i\}$ , where  $i = 1 : 6$  for the 3D case),  $\{\chi_e^i\}$  is the displacement vector of the element ( $e$ ) corresponding to the application of the volumetric strain field  $\{\epsilon^i\}$  and  $\{\chi_e^{0(i)}\}$  is the displacement vector of the ( $e$ ) element corresponding to the macroscopic strain field  $\{\epsilon^{0i}\}$ . The 2D

and 3D numerical implementation of the homogenization process are provided in [Andreassen & Andreassen \(2014\)](#) and [Guoying et al. \(2018\)](#), respectively.

### 3.3. Homogenization of the microstructures' unit cell configurations

Different configurations of the same microstructure type result to different homogenized properties. [Figure 4](#) depicts intermediate configurations of the elementary microstructure types along with their homogenized elasticity tensor, corresponding to intermediate values of their geometric parameter vector. A regression analysis is performed in order to model the variation in the homogenized mechanical property with respect to the geometric configuration for each microstructure type. The parameters representing the geometric configurations in the regression analysis process will constitute the design variables for the HTOP, and are selected based on the computational effect they bear on the HTOP. The criteria for their selection are discussed in the following section.

Regardless of the type of design variables determined for the HTOP, the regression model to be fitted depends mainly on three parameters: **(1)** the length of each microstructure's geometric parameter vector, which is dependent on the discretization mesh set for its unit cell, **(2)** the deviation in the mechanical properties between the *material*<sub>1</sub> and *material*<sub>2</sub> components; that is, material components of similar mechanical properties, say  $[\lambda_1, \mu_1] \approx [\lambda_2, \mu_2]$ , will result in small variations in the calculated homogenized elasticity tensors, while in case of material components of significant difference in their mechanical properties, a more complex regression model might be required, and **(3)** the variation in the homogenized property with respect to the microstructure's configuration. Depending on those parameters, different regression models may deem more adequate among others, and different fitting quality metrics such as the  $R^2$ , the average and maximum relative error, (ARE) and (MRE) respectively, can be employed to identify the best amongst them.

Since the scope of this work is to generalize the mathematical framework of the proposed methodology, independent of the candidate microstructures and their material components, no emphasis to optimizing with respect to the regression model will be given in this work. Further, the proposed developments are independent from the selected regression model.

#### 3.3.1. Determining the design variables for the HTOP

In the present case study where two-component microstructures are considered, and with the volume constraint concerning the *material*<sub>1</sub> component, two types of design variables are distinguished for the HTOP. Each type poses the HTOP differently, and bears a different effect both on its computational efficiency and accuracy in the results obtained:

**(1)** The first approach would be to consider the geometric parameters of the microstructures as the design variables for the HTOP. By that means, the volume constraint imposed on *material*<sub>1</sub> is given as a explicit function of the

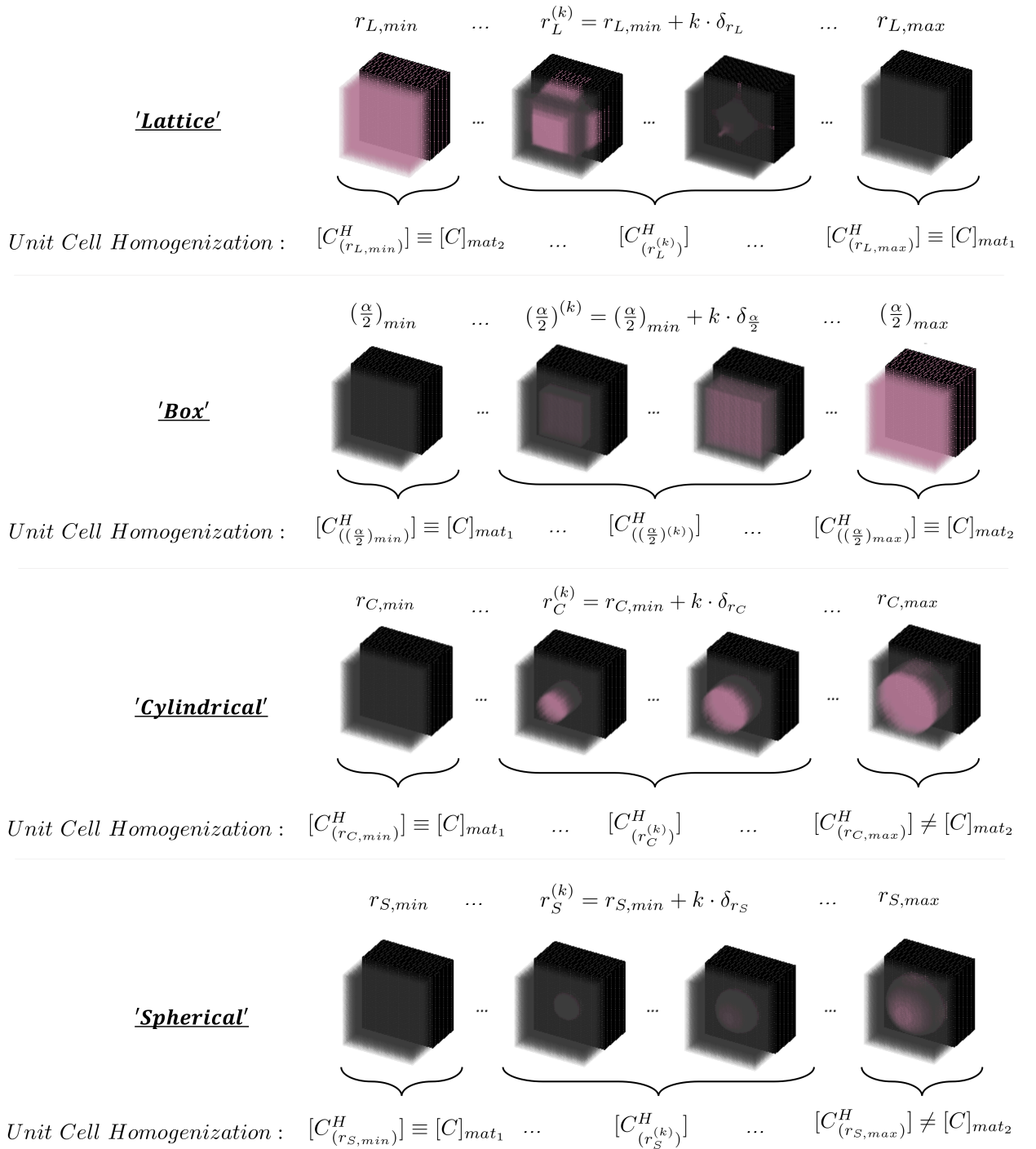


**Figure 4:** Homogenizing the elasticity tensor of the intermediate configurations of the four microstructures. The superscript  $(k)$  refers to the intermediate configurations of the microstructures, *i.e.* at  $p^{(k)} = [r_L^{(k)}; (\frac{\alpha}{2})^{(k)}; r_C^{(k)}; r_S^{(k)}]$ . Note that, at the extreme values of their geometric parameters only for the 'Lattice' and 'Box' microstructures the pure  $material_1$  and  $material_2$  mechanical properties are derived.

microstructures' geometric parameters. This approach also suggests that the regression process discussed in the previous section, is performed between the homogenized elasticity tensor and the geometric parameter for each microstructure, *i.e.* the regression models to be fitted are of the form  $C_{ij(r_L)}^H, C_{ij(\frac{\pi}{2})}^H, C_{ij(r_C)}^H, C_{ij(r_S)}^H$ , with  $(i, j) = 1 : 6$ . Any large variations in the order of magnitudes among the HTOP constraints constitute a numerical shortcoming for this approach. This occurs especially in case the design variables are order of magnitudes less than zero, as in the present case where the order of magnitude is defined by the scale ratio  $\epsilon$  (the design variables are defined in the micro-scale). As a result, constraints low in magnitude are neglected in the numerical calculations. The standard approach to minimize the impact of large variations in magnitudes among the constraints is to scale (or normalize) either the constraint functions or the design variables, which leads to the approach discussed next.

(2) Establishing the monotonicity between the  $material_1$  volume and the microstructures geometric parameters, the more computationally efficient approach would be to consider the  $material_1$  volume fraction of the microstructures as the design variables for the HTOP; that is, optimize their topology with respect to the dimensionless ratios  $v_{type}^{(k)} = \frac{V_{type}^{(k)}}{V_{uc}} \in [v_{type,min}, v_{type,max}]$ . Here, the subscript *type* indicates the type of the microstructure, where  $type \in \mathcal{T} = \{ 'L', 'B', 'C', 'S' \}$ . The numerator of the fraction  $V_{type}^{(k)}$ , is the  $material_1$  volume within the constant unit cell volume  $V_{uc}$  corresponding at its ( $k^{th}$ ) unit cell configuration, *i.e.* at the ( $k^{th}$ ) element of its geometric parameter vector (see Figure 4), and  $v_{type,\{min,max\}}$  is the minimum and maximum volume ratio  $material_1$  can occupy within  $V_{uc}$ . The bounds of the  $material_1$  volume fraction for the four microstructures are listed in Table 2. This approach suggests that the regression process takes place between the homogenized tensor of the microstructures and their  $material_1$  volume fraction, *i.e.* the four regression models are of the form  $C_{ij(v_L)}^H, C_{ij(v_B)}^H, C_{ij(v_C)}^H, C_{ij(v_S)}^H$ , with  $(i, j) = 1 : 6$ . Through these regression models the candidate microstructures are represented in the catalogue. An additional advantage that comes with this approach, beyond that of ending up with scaled side constraints for the HTOP, is that it significantly simplifies the mathematical formulation of the volume constraint imposed on the  $material_1$  (discussed in detail in (Sec. 5.3)). For these reasons, the  $material_1$  volume fractions of the individual microstructures are selected as the design variables for the HTOP. The regression models selected for fitting the homogenized elasticity tensors to the different  $material_1$  volume fractions are presented along with the numerical examples in (Sec. 6).

Table 2: Bounds of the  $material_1$  volume fraction for each microstructure type [-]

$v_{L,min} = 10^{-9} \leq \overbrace{\{v_L\}}{'Lattice'} \leq v_{L,max} = 1$
$v_{B,min} = 10^{-9} \leq \overbrace{\{v_B\}}{'Box'} \leq v_{B,max} = 1$
$v_{C,min} = 0.2146 \leq \overbrace{\{v_C\}}{'Cylindrical'} \leq v_{C,max} = 1$
$v_{S,min} = 0.4764 \leq \overbrace{\{v_S\}}{'Spherical'} \leq v_{S,max} = 1$

For notational convenience, and since the scope of this work is to generalize the mathematical framework of the SFP-based HTDMOP for the case of  $2^k$  candidate microstructures, the numerical index notation is adopted from now onwards. The notation takes the following form for the four microstructures :  $\{v_L, v_B, v_C, v_S\} \rightarrow \{v_1, v_2, v_3, v_4\}$

#### 4. Interpolating the homogenized properties by means of the DMO technique

Discrete material optimization (DMO) is a technique developed for purposes of material optimization from a list of pre-defined candidate materials (Stegmann & Lund (2005); Stegmann (2004)). DMO proposes the following scheme for the interpolation of the mechanical properties of  $n_c$  candidate materials within the ( $e$ ) element:

$$[C_{e\{w_e\}}] = \sum_{i=1}^{n_c} W_{ei} \cdot [C_i], \quad \text{where, } W_{ei} = (w_{ei}^p \cdot \prod_{\substack{j=1 \\ j \neq i}}^{n_c} (1 - w_{ej})^p) \quad \text{and} \quad 0 \leq w_{ei} \leq 1, \quad (3)$$

where,  $W_{ei}$  is the weight assigned to the ( $i^{th}$ ) candidate material,  $[C_i]$  its constant elasticity tensor, and  $p \in \mathbb{R}^+$  a penalty factor forcing intermediate values of the weights closer to their  $\{0, 1\}$  bounds. The goal of the DMO-based MOP is to solve for the  $W_{ei}$  weights and identify a unique material for each element in the domain.

Adopting the DMO scheme to interpolate the homogenized elasticity tensors of  $n_c$  candidate microstructures within the ( $e$ ) element, Eq.(3) reads:

$$[C_{e(\{w_e\}, \{v_e\})}^H] = \sum_{i=1}^{n_c} W_{ei} \cdot [C_{i(v_{ei})}^H], \quad \text{where, } W_{ei} = (w_{ei}^p \cdot \prod_{\substack{j=1 \\ j \neq i}}^{n_c} (1 - w_{ej})^p) \quad \text{and} \quad 0 \leq w_{ei} \leq 1, \quad (4)$$

where the weight  $W_{ei}$  corresponds now to the ( $i^{th}$ ) in order candidate microstructure of  $v_{ei}$  *material*<sub>1</sub> volume fraction, and  $[C_{i(v_{ei})}^H]$  its homogenized elasticity tensor, as derived from the regression process discussed previously. The curly bracket notation is adopted in Eqs.(3)-(4) to represent all weights  $W_{ei}$  and *material*<sub>1</sub> volume fractions  $v_{ei}$  in a vector format.

The corresponding DMO-based HTDMOP is optimized with respect to the weights  $\{w_e\}$  and the *material*<sub>1</sub> volume fractions  $\{v_e\}$  of each element ( $e$ ) in the structural domain. The microstructure type predicted for the element is determined solely by the optimal  $\{w_e\}^*$  vector. Its configuration is determined by applying the DMO interpolation scheme on the predicted *material*<sub>1</sub> volume fractions  $\{v_e\}^*$ , as such it is dependent on both the  $\{w_e\}^*$  and the  $\{v_e\}^*$  design variables.

The DMO technique proves to be a very efficient approach when applied on small scale material optimization problems. However, when considering either a dense mesh for the structure and a short list of candidate materials assigned per element/patch or a coarse mesh for the structure and an extensive list of candidate materials, the dimension

of the resulting MOP still remains large. This one-to-one dependency of the DMO-based MOP dimension on both the number of design variables assigned per element/patch in the structural domain and the discretization mesh set, renders the resulting optimization problem quite challenging and computationally expensive. For this purpose, the SFP method is considered in this study as the weight assignment method for the candidate microstructures.

## 5. Formulation of the SFP-based HTDMOP

The scope of this section is to formulate the SFP-based HTDMOP for compliance minimization of the structure. The section is structured as follows: in (Sec. 5.1) an overview of the SFP material interpolation technique is given. Following, the SFP technique is employed for interpolating the candidate homogenized properties within each element ( $e$ ) of the structural domain. In (Sec. 5.2), the stiffness matrix and its Jacobian are derived for the ( $e$ ) element. In (Sec. 5.3) the generalized SFP-based HTDMOP for compliance minimization of the structure is posed. Further, the way it can be perceived as a concurrent homogenization-based topology, multi-material and/or microstructure type optimization problem is presented.

### 5.1. Interpolating the homogenized properties by means of the SFP technique

As an alternative to the DMO technique, the shape function with penalization method (SFP) has been proposed in Bruyneel et al. (2011) and Bruyneel (2011). This approach utilizes the shape functions of the  $2^k$ -noded quadrangular FE as weights for the candidate materials: Each candidate material is tied to a specific node on the quadrangular FE, and the solution is optimized with respect to the nodal coordinates configuration. By that means, the number of design variables is reduced to one for the case of two candidate materials per element in the domain (use of the 1D linear FE), to 2 for 4 candidate materials (use of the 2D quadrilateral FE), to 3 for 8 (use of the hexahedral FE), and to  $k$  for the general case of  $2^k$  candidate materials, with  $k \in \mathbb{N}^+$ . The shape functions of the  $2^k$ -noded quadrangular FE are given by the product:

$$N_{i(\xi_{j=1:k})} = \frac{1}{2^k} \cdot \left( \prod_{j=1}^k (1 + \xi_j \cdot \xi_{ji}) \right) \quad \text{with } i = 1 : 2^k, \quad (5)$$

where  $\xi_j$  is the ( $j^{\text{th}}$ ) natural coordinate of the  $2^k$ -noded quadrangular FE and  $\xi_{ji}$  are the coordinates of the ( $i^{\text{th}}$ ) node in the ( $j^{\text{th}}$ ) direction. Since the design variables of the resulting SFP-based MOP are the natural coordinates of the  $2^k$ -noded quadrangular FE, their side constraints are defined within the  $k$ -dimensional hyperrectangle  $[-1, 1]^k$ .

For the general case of  $2^k$  candidate materials, SFP proposes the following interpolation scheme:

$$[C_{e(\{\xi_e\})}] = \sum_{i=1}^{2^k} N_{ei(\{\xi_e\})}^p \cdot [C_i], \quad (6)$$

where  $\{\xi_e\}$  are the natural coordinates of the  $2^k - \text{noded}$  quadrangular FE expressed in a vector format, *i.e.*  $\{\xi_e\} = [\xi_{e1}, \xi_{e2}, \dots, \xi_{ek}] \in [-1, 1]^k$ ,  $N_{ei(\{\xi_e\})}$ , the shape function corresponding to the ( $i^{\text{th}}$ ) node, and  $[C_i]$  the elasticity tensor tied to it. The penalty factor  $p$  forces the shape functions  $N_{e(\{\xi_e\})}$  towards their  $\{0, 1\}$  bounds so as to ensure that a unique material is predicted for the element. The penalty factor can be set equal to 1, as in the classical FEM scheme or be assigned values  $p \geq 3$ . Depending on the value assigned to  $p$  there is a trade-off between achieving a high computational efficiency and forcing convergence towards a discrete solution (discussed in detail in (Sec. 5.3)). **Figure 5** illustrates the SFP interpolation scheme in the case where four and eight candidate materials are considered per element ( $e$ ) in the structural domain.

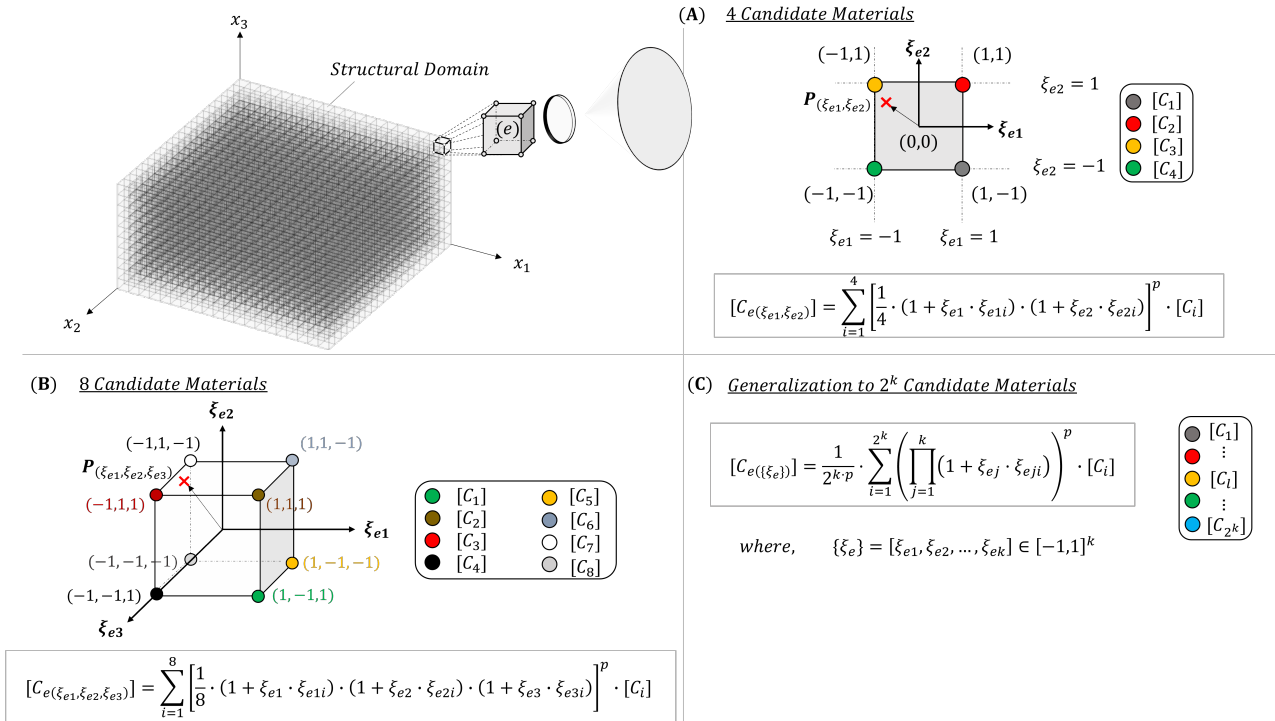


**Figure 5:** Illustration of the SFP material interpolation technique: **(A)** Each of the 4 candidate materials is assigned to a nodal location  $(\xi_{e1i}, \xi_{e2i})$  on the quadrilateral FE, with  $i = 1 : 4$ ; the optimal coordinate  $P_{(\xi_{e1}, \xi_{e2})} \in [-1, 1]^2$  is sought. **(B)** Each of the 8 candidate materials is assigned to a nodal coordinate  $(\xi_{e1i}, \xi_{e2i}, \xi_{e3i})$  on the hexahedral FE, with  $i = 1 : 8$ ; the optimal coordinate  $P_{(\xi_{e1}, \xi_{e2}, \xi_{e3})} \in [-1, 1]^3$  is sought. **(C)** Generalization of the SFP technique for the case of  $2^k$  candidate materials; here, the optimal coordinate  $P_{(\xi_{e1}, \dots, \xi_{ek})} \in [-1, 1]^k$  is sought. (For convenience, the analytical expression of the element's elasticity tensor is included for each case.)

Adopting the SFP scheme to parametrize the homogenized elasticity tensors of  $2^k$  candidate microstructures within the ( $e$ ) element, Eq.(6) reads:

$$[C_{e(\{\xi_e\}, \{v_e\})}^H] = \sum_{i=1}^{2^k} N_{ei(\{\xi_e\})}^p \cdot [C_{i(v_{ei})}^H]. \quad (7)$$

As stated in Eq.(7), the elasticity tensor of the ( $e$ ) element is dependent both on the type of the candidate microstructures, now determined by the coordinates of the  $\{\xi_e\}$  vector, and the individual  $material_1$  volume fractions  $\{v_e\}$ . For notational brevity, the  $\{\xi_e\}$  and  $\{v_e\}$  vectors of the ( $e$ ) element are collected in a unique vector denoted as  $\{dv\}_e = [\{\xi_e\}, \{v_e\}]$ . The *dimension* of the  $\{dv\}_e$  vector for the general case when  $2^k$  candidate microstructures are considered for the element, equals to:  $dim(\{dv\}_e) = dim(\{\xi\}_e) + dim(\{v\}_e) = k + 2^k$ . Thus, for a structural domain discretized in  $N$  number of FEs, with each element bearing its own microstructure, the optimal solution  $\{dv\}^*$  lies within the  $\mathbb{R}^{(k+2^k) \cdot N}$  Euclidean space, *i.e.*  $\{dv\}^* = \bigcup_{e=1}^N \{dv\}_e^* \in \mathbb{R}^{(k+2^k) \cdot N}$ .

Figures 6 & 7 demonstrate the way in which the SFP technique is employed to interpolate the homogenized elasticity tensors of the candidate microstructures within the ( $e$ ) element. For instance, considering the case of two candidate microstructures, as shown Figure 6(A), each of them is assigned to a node on the 1D linear FE. In this case, the optimal of the two is determined by the optimal coordinate  $\xi_e^* \in [0, 1]$ . The homogenized elasticity tensors of both microstructures are dependent on their  $material_1$  volume fraction, denoted as  $v_{e1}$  and  $v_{e2}$ , respectively. The  $\xi_e$  natural coordinate along with the  $v_{e1}$  and  $v_{e2}$  volume fractions of the two microstructures form the design variable vector for the ( $e$ ) element, *i.e.*  $\{dv\}_e = [\xi_e, v_{e1}, v_{e2}]$ . Considering now the case of four candidate microstructures, as shown in Figure 7(A), each of them is assigned to a specific node on the 2D quadrangular FE. In this case, the design variable vector of the ( $e$ ) element is defined as  $\{dv\}_e = [\xi_{e1}, \xi_{e2}, v_{e1}, v_{e2}, v_{e3}, v_{e4}]$ , and the optimal natural coordinate lies within the quadrangular FE, *i.e.*  $\{\xi_e\}^* = (\xi_{e1}, \xi_{e2})^* \in [-1, 1]^2$  - ideally, exactly on one of the nodes of the FE-. Figures 7B & 8 illustrate the way in which the microstructure type optimization problem can be combined with the multi-material optimization problem by simply assigning to the nodes of the FE both different microstructure types of the same two material components and microstructures of the same type but of different  $material_2$  components. In this case, the basic precondition is that the homogenized properties of the latter are also expressed in terms of their  $material_1$  volume fractions. For convenience, the design variable vector of the ( $e$ ) element  $\{dv\}_e$  and the analytical expression of its elasticity tensor  $[C_{e(\{dv\}_e)}^H]$  are included in the figures.

In their original work (Bruyneel (2011)), the authors also examined the case where three candidate materials are considered for the domain. In this case, the shape functions of the 2D triangular FE were employed as weights for the candidate materials. An additional inequality constraint ensuring that the optimal natural coordinate  $\{\xi_e\}^*$  lies within the orthogonal triangle is imposed per element ( $e$ ) in the structural domain. In particular, it constraints the solution  $\{\xi_e\}^* = (\xi_{e1}, \xi_{e2})^*$  to lie within the feasible domain  $\mathcal{S} = \{\{\xi_e\} \in \mathbb{R}^2 \mid 0 \leq \{\xi_e\} \leq 1, g_e : \xi_{e1} + \xi_{e2} - 1 \leq 0\}$ , as depicted in Figure 6(B). To comply with their work, the formulation of the SFP-based HTDMOP for the case of three candidate microstructures is also listed in (Sec. 5.3).

It is noted that, both the SFP-based MOP and the DMO-based MOP constitute problems of non-linear Discrete Optimization (DP). However, due to the computational intensiveness of the non-linear DP, the common approach is to

relax that constraint and treat the design variables as continuous within the design space. After the continuous solution is found it is rounded to the nearest feasible discrete design. For the SFP-based MOP, this translates to rounding the solution to the nearest vertex of the  $k$ -dimensional hyperrectangle.

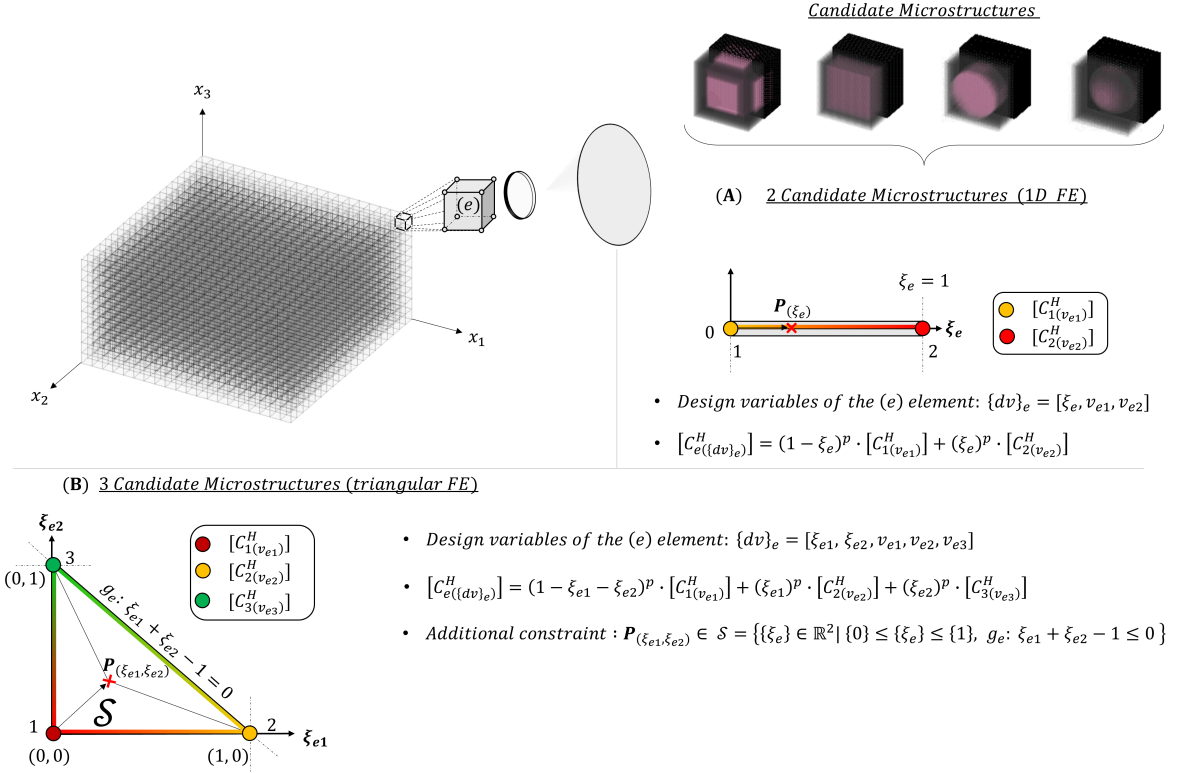


**Figure 6:** (A) The shape functions of the 1D linear FE are employed as weights for the case of two candidate microstructures. (B) The shape functions of the orthogonal triangular FE are employed as weights for the case of three candidate microstructures. The optimal coordinate  $P^* = \{\xi_e^*\}$  lies within the feasible domain  $S$ .

## 5.2. Derivation of the element's stiffness matrix

The stiffness matrix of the  $(e)$  element is expressed as follows:

$$\begin{aligned}
 [K_{e(\{dv\}_e)}] &= \int_{V_E} [B_e]^T \cdot \left( \sum_{i=1}^{2^k} N_{ei(\{\xi_e\})}^p \cdot [C_{i(v_{ei})}^H] \right) \cdot [B_e] dV = \sum_{i=1}^{2^k} N_{ei(\{\xi_e\})}^p \cdot \left( \int_{V_E} [B_e]^T \cdot [C_{i(v_{ei})}^H] \cdot [B_e] dV \right) \\
 &= \sum_{i=1}^{2^k} N_{ei(\{\xi_e\})}^p \cdot [K_{ei(v_{ei})}], \tag{8}
 \end{aligned}$$

where  $[K_{ei(v_{ei})}]$  is the  $[24 \times 24]$  stiffness tensor of the  $(i^{th})$  in order candidate microstructure of  $v_{ei}$  material<sub>1</sub> volume fraction,  $V_E$  is the volume of the element and  $[B_e]$  is the  $[6 \times 24]$  Jacobian matrix of the element's shape functions.

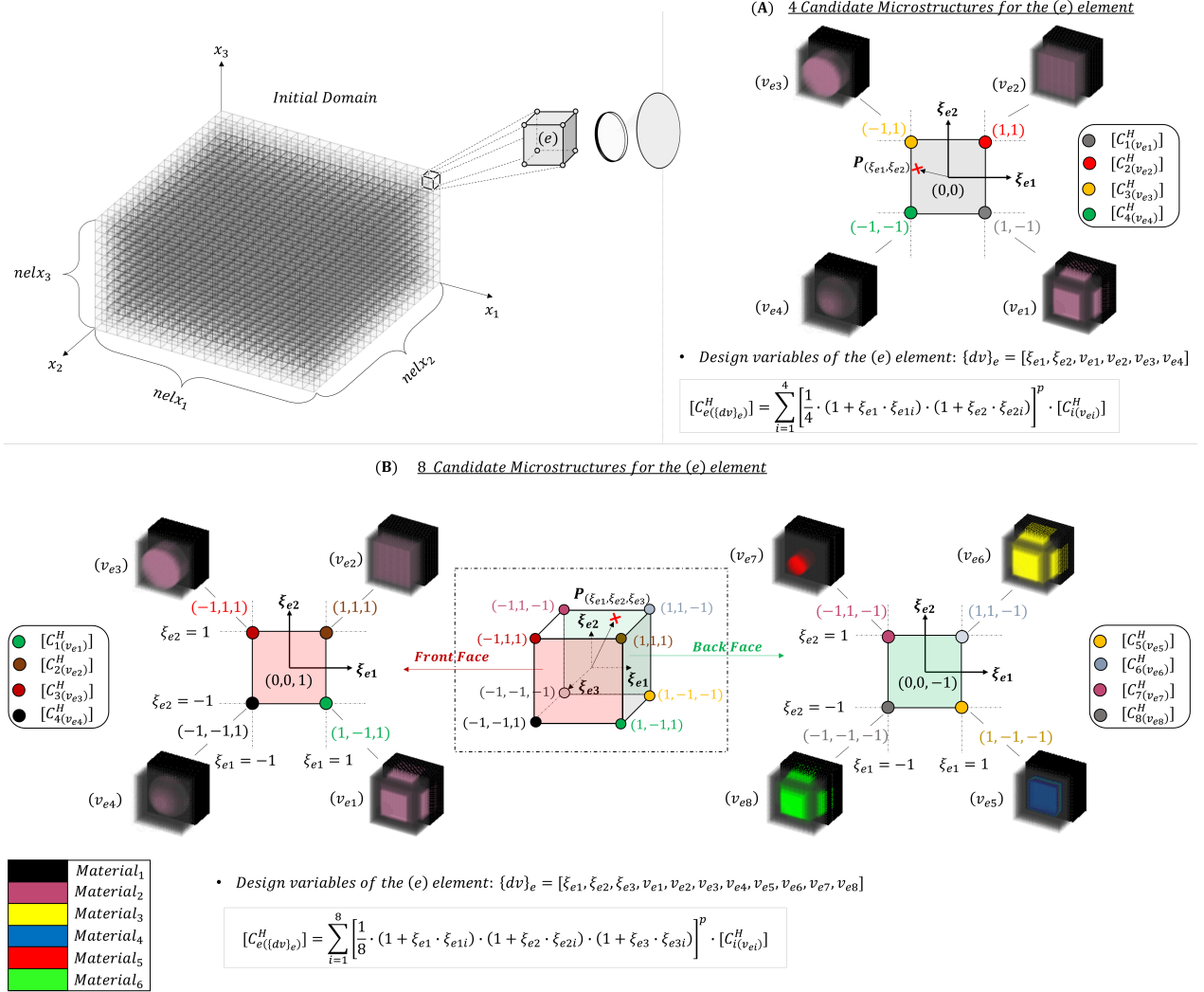


**Figure 7: (A)** The shape functions of the quadrilateral FE are employed as the weights for the 4 candidate microstructures. The optimal coordinate  $P_{(\xi_{e1}, \xi_{e2})} \in [-1, 1]^2$  is sought. **(B) (a)** The shape functions of the hexahedral FE are employed as the weights for the 8 candidate microstructures. The optimal coordinate  $P_{(\xi_{e1}, \xi_{e2}, \xi_{e3})} \in [-1, 1]^3$  is sought. **(b)** The methodology allows for the alternation or combination between the microstructure type and the multi-material optimization problem, e.g. different microstructure types of the same material components are allocated to the nodes of the **Front Face** of the hex element, and different microstructure types of different 'material'<sub>2</sub> components at the nodes of its **Back Face**.

### 5.2.1. Calculating the Jacobian of the (e) element's stiffness matrix

The derivative of the (e) element's stiffness matrix is split in two parts: one *w.r.t* to the components of the  $\{\xi_e\}$  design variable vector:

$$\frac{d[K_{e((dv)_e)}]}{d\xi_{ej}} = \sum_{i=1}^{2k} \frac{dN_{ei}^p}{d\xi_{ej}} \cdot [K_{ei(v_{ei})}] \quad \text{with } j = 1 : k, \quad (9)$$

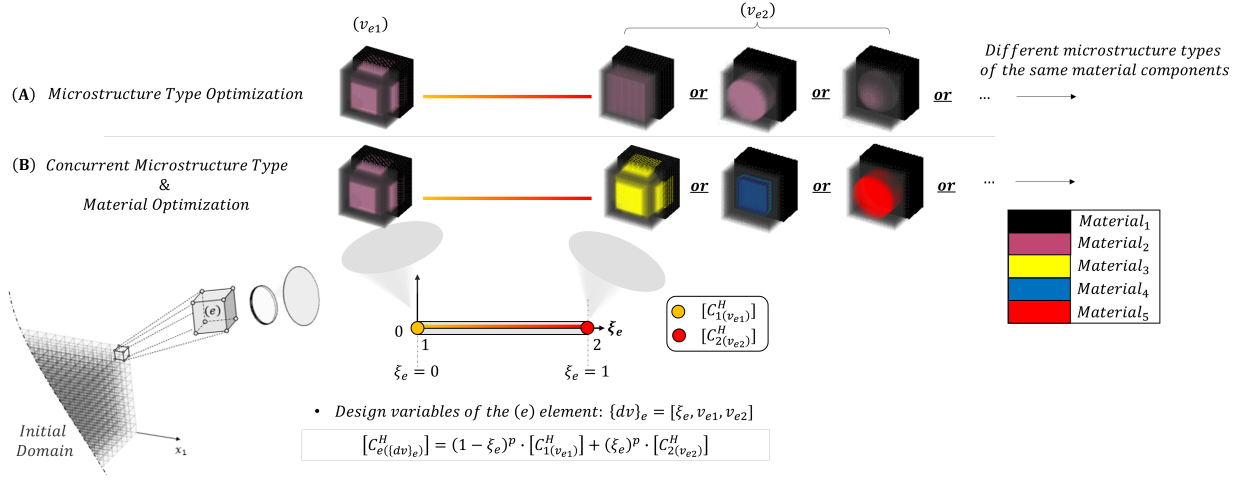


**Figure 8:** (A) Optimizing with respect to the microstructure type. (B) Optimizing with respect to both the microstructure type and the 'material' component.

and one with respect to the components of the  $\{v_e\}$  design variable vector:

$$\frac{d[K_{e(\{dv\}_e)}]}{dv_{ei}} = N^p_{ei(\{\xi_e\})} \cdot \left( \int_{V_e} [B_e]^T \cdot \frac{d[C^H_{i(v_{ei})}]}{dv_{ei}} \cdot [B_e] dV \right) \quad \text{with } i = 1 : 2^k. \quad (10)$$

### 5.3. Posing the SFP-based HTDMOP for the general case of $2^k$ candidate microstructures

The common practice in static linear TO is to optimize the compliance of the structural domain. The compliance minimization problem is subjected to the system's equilibrium equations, the volume constraint imposed on the isotropic material, and the side constraints of the relative densities. Similarly is posed the SFP-based HTDMOP for compliance minimization, under the following two differences: (1) the volume constraint is now imposed on one of the constituent materials of the candidate microstructures, and (2) the additional constraint of Eq.(14) is imposed as to enforce the self-complementary property on the penalized shape functions. For the general case of  $2^k$  candidate microstructures, and with the volume constraint assumed on the *material*<sub>1</sub> component, the SFP-based HTDMOP for compliance minimization is posed as follows:

$$\{dv\}^* = \underset{\{dv\} \in \mathbb{R}^{N \cdot (k+2^k)}}{\operatorname{argmin}} \quad C = \sum_{e=1}^N \{U_{e(\{dv\}_e)}\}^T \cdot [K_{e(\{dv\}_e)}] \cdot \{U_{e(\{dv\}_e)}\} \quad (11)$$

**s.t.**

$$\bullet [K_{all}] \cdot \{U_{all}\} = \{F_{all}\} \Rightarrow \{H\} : \left( \sum_{e=1}^N [K_{e(\{dv\}_e)}] \cdot \{U_{e(\{dv\}_e)}\} \right) - \{F_{all}\} = \{0\}, \quad (12)$$

- $\frac{V_{material_1}}{V_0} \leq f_{volfrac}^1 \Rightarrow F_{(\{dv\})} : \frac{\sum_{e=1}^N \sum_{i=1}^{2^k} N_{ei(\{\xi_e\})}^p \cdot v_{ei}}{N \cdot f_{volfrac}^1} - 1 \leq 0,$  (13)

- $h_{e(\{\xi_e\})} : \sum_{i=1}^{2^k} N_{ei(\{\xi_e\})}^p - 1 = 0 \quad \text{with } e = 1 : N,$  (14)

- $\{dv\}_{e,min} \leq \{dv\}_e \leq \{dv\}_{e,max} \quad \text{with } e = 1 : N,$  (15)

with,

- $\{dv\}_{e,min} = \underbrace{[-1, -1, \dots, -1]}_{1 \times k}; \underbrace{v_{e1,min}, v_{e2,min}, \dots, v_{e2^k,min}}_{1 \times 2^k} \quad \text{with } e = 1 : N,$  (16)

- $\{dv\}_{e,max} = \underbrace{[1, 1, \dots, 1]}_{1 \times (2^k + k)} \quad \text{with } e = 1 : N,$  (17)

where  $\{dv\}_e$  is the design variable vector of the ( $e$ ) element,  $N$  is the number of the equally-sized FEs discretizing the structural domain,  $[K_{all}]$  is the global stiffness matrix,  $\{F_{all}\}$  is the external load vector (considered independent of the design variables, i.e.  $\frac{dF_{allj}}{d(\{dv\}_e)} = 0_{j \times N \cdot (k+2^k)}$ , with  $j = 1 : ndofs$  and  $ndofs$  the degrees of freedom of the domain),  $\{U_{all}\}$  is the global displacement vector,  $\{U_{e(\{dv\}_e)}\}$  the nodal displacement vector of the ( $e$ ) element,  $K_{e(\{dv\}_e)}$  its stiffness matrix,  $V_{material_1}$  is the total volume of  $material_1$  within the domain,  $f_{volfrac}^1$  is the fraction of the allowable total  $material_1$  volume to the volume of the initial domain  $V_0$ , and  $\{dv\}_{e,min}$  and  $\{dv\}_{e,max}$  are the side constraints of the  $\{dv\}_e$  design variable vector (same for all  $N$  elements in the structural domain).

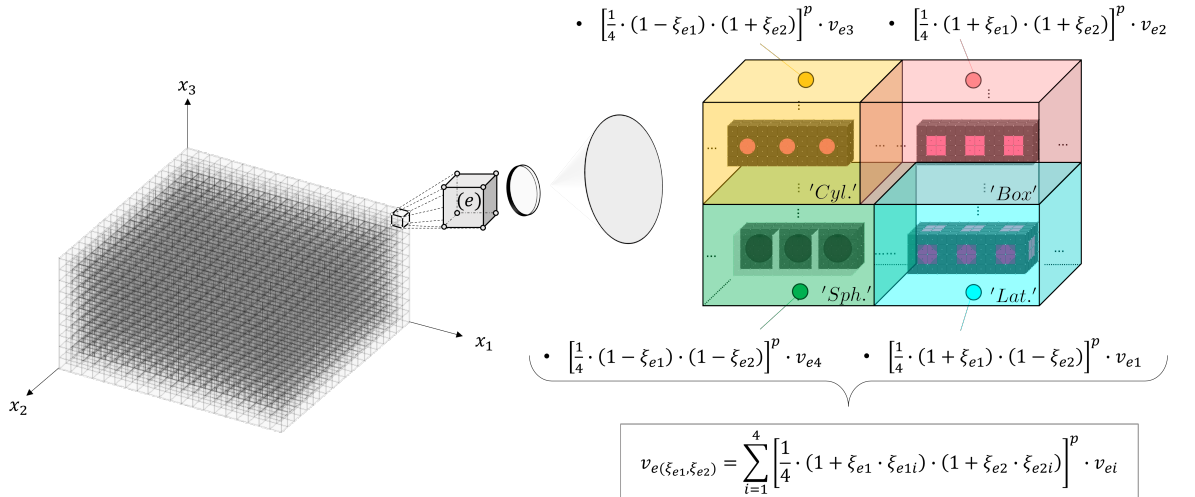


**Figure 9:** Elaboration on the volume constraint of Eq.(13): Examining the case where the four elementary microstructure types are considered for the ( $e$ ) element, the total  $material_1$  volume fraction within it  $v_e$ , is calculated by implementing the SFP interpolation scheme on the  $material_1$  volume fractions of the individual microstructures. The fraction occupied by each microstructure type within the element is determined by the numerical value of the (penalized) shape function tied to it (depicted as the individual colored blocks in the figure).

The equality constraint set of Eq.(14) is present only when  $p \neq 1$ . Indeed, when the penalty factor is set equal to unity, the equality constraint set is automatically satisfied due to the self-complementary property of the shape functions  $N_{ei(\{\xi_e\})}$  in the  $[-1, 1]^k$  domain, expressed as follows:  $\sum_{i=1}^{2^k} N_{ei(\{\xi_e\})} = 1, \forall \{\xi_e\} \in [-1, 1]^k$ . When  $p \in \mathbb{R}_{\neq 1}^+$ , the equality constraint must hold for all elements in the domain. However, the effect of the penalty factor value is not limited to the imposition of  $N$  additional equality constraints on the optimization problem, as it also affects the degree of non-convexity in the design functions; the higher the penalty factor value is set the higher the degree of non-linearity of the design functions, rendering standard gradient-based solution algorithms such as MMA (Svanberg (1987)), insufficient for such optimization problems (since the solution might get trapped in strong local minima within the design space). To generalize the expression of the equality constraint set, the  $p$  value condition is introduced as a Boolean operator ( $p \neq 1$ ), (de-)activating the constraints depending on its value. By that means, Eq.(14) is modified as follows:

$$h_{e(\{\xi_e\})}^* : (p \neq 1) \cdot \left( \sum_{i=1}^{2^k} N_{ei(\{\xi_e\})}^p - 1 \right) = 0 \quad \text{with } e = 1 : N. \quad (18)$$

The above Boolean expression is true when  $p \neq 1$  and false when  $p = 1$ . Since  $p$  is independent of the design variables, the Jacobian of the initial equality constraint set is simply multiplied by the operator.

Table 3: Posing the SFP-based HTDMOP for the cases of 2, 3 and 4 candidate microstructures

$$\{dv\}^* = \underset{\{dv\} \in \mathbb{R}^{N \cdot (k+2k)}}{\operatorname{argmin}} C = \sum_{e=1}^N \{U_{e(\{dv\}_e)}\}^T \cdot [K_{e(\{dv\}_e)}] \cdot \{U_{e(\{dv\}_e)}\}$$

s.t.

$$\bullet \{H\}: \left( \sum_{e=1}^N [K_{e(\{dv\}_e)}] \cdot \{U_{e(\{dv\}_e)}\} \right) - \{F_{all}\} = \{0\},$$

where,

	2 Microstructures	3 Microstructures	4 Microstructures
$\{dv\}_e :$	$[\xi_e, v_{e1}, v_{e2}]$	$[\xi_{e1}, \xi_{e2}, v_{e1}, v_{e2}, v_{e3}]$	$[\xi_{e1}, \xi_{e2}, v_{e1}, v_{e2}, v_{e3}, v_{e4}]$
$F_{(\{dv\})} :$	$\frac{\sum_{e=1}^N \left( (1-\xi_e)^p \cdot v_{e1} + \xi_e^p \cdot v_{e2} \right)}{N \cdot f_{vol frac}^1} - 1$	$\frac{\sum_{e=1}^N \left( (1-\xi_{e1}-\xi_{e2})^p \cdot v_{e1} + \xi_{e1}^p \cdot v_{e2} + \xi_{e2}^p \cdot v_{e3} \right)}{N \cdot f_{vol frac}^1} - 1$	$\frac{\sum_{e=1}^N \left( \sum_{i=1}^4 \left[ \frac{1}{4} \cdot (1+\xi_{e1} \cdot \xi_{e1i}) \cdot (1+\xi_{e2} \cdot \xi_{e2i}) \right]^p \cdot v_{ei} \right)}{N \cdot f_{vol frac}^1} - 1$
$(*) h_{e(\{\xi_e\})} :$	$\left( (1-\xi_e)^p + \xi_e^p \right) - 1$	$\left( (1-\xi_{e1}-\xi_{e2})^p + \xi_{e1}^p + \xi_{e2}^p \right) - 1$	$\sum_{i=1}^4 \left[ \frac{1}{4} \cdot (1+\xi_{e1} \cdot \xi_{e1i}) \cdot (1+\xi_{e2} \cdot \xi_{e2i}) \right]^p - 1$
$(*) (*) g_{e(\{\xi_e\})} :$		$\xi_{e1} + \xi_{e2} - 1$	
$(*) \{dv\}_{e,min} :$	$[0, v_{e1,min}, v_{e2,min}]$	$[0, 0, v_{e1,min}, v_{e2,min}, v_{e3,min}]$	$[-1, -1, v_{e1,min}, v_{e2,min}, v_{e3,min}, v_{e4,min}]$
$(*) \{dv\}_{e,max} :$	$[1, v_{e1,max}, v_{e2,max}]$	$[1, 1, v_{e1,max}, v_{e2,max}, v_{e3,max}]$	$[1, 1, v_{e1,max}, v_{e2,max}, v_{e3,max}, v_{e4,max}]$

(\*) The constraint holds for each element (e) in the domain

(\*) (\*) The vector-valued inequality constraint set can be converted into a scalar-valued function by means of the K-S function (Wrenn (1989))

## 6. Numerical examples

The academic case studies of the 3D cantilever and the MBB beams constitute the extension of the 2D numerical examples initially presented in Sigmund (2001) and Andreassen et al. (2011), and their numerical implementation

for the standard TOP in MATLAB can be found in [Liu & Tovar \(2014\)](#). In this section the developed methodology is demonstrated on two different numerical examples for the case study of the 3D MBB beam. The first example examines the case where the '*Cylindrical*' microstructure of two candidate fiber (inner cylinder) orientations is considered for the MBB beam. The main goal of this example is to emphasize that the methodology need not necessarily be tied to the microstructure type optimization problem and that it can be implemented as is in different classes of optimization problems. The second test example examines the case where all four microstructure types discussed thus far are considered as candidates for the MBB beam. Here, the issue concerning the level of discreteness in the final design raises and different alternatives for tackling it are presented.

The design parameters are set the same for both numerical examples: the MBB beam is simply supported on its lower edges with a vertical unit point load oppositely directed to the  $x_3$  axis being applied at the middle of the bottom face. The beam follows a  $[40 \times 40 \times 20]$  discretization mesh along the  $x_1$ ,  $x_2$  and  $x_3$  axis, respectively, and the scale ratio has been set equal to  $\epsilon_i = 10^{-3}$  per direction  $i \in \{1, 2, 3\}$ .

The mechanical properties of the two material components are set equal to  $\lambda_1 = 5.769$  and  $\mu_1 = 3.846$  for *material*<sub>1</sub> and  $\lambda_2 = 5.769 \cdot 10^{-2}$  and  $\mu_2 = 3.846 \cdot 10^{-2}$  for *material*<sub>2</sub>, and are kept the same in all test examples. The three-parameter *sigmoid* function proved to be the most suitable for fitting the homogenized properties to the *material*<sub>1</sub> volume fractions for all microstructure types, providing an adjusted  $R_{type}^2 \simeq 1$  (the *sigmoid* model displayed a slightly higher  $R_{type}^2$  than the standard uni-variate *cubic* polynomial that was initially considered). [Figure 10](#) depicts the *sigmoid* fit for all terms of the homogenized elasticity tensor of the '*Lattice*' microstructure. The forward finite difference (FFD) method has been implemented to calculate the first order derivatives of the homogenized elasticity tensor with respect to the *material*<sub>1</sub> volume fraction for each microstructure. The increment step set per iteration ( $k$ ) in the FFD process for each microstructure ( $i$ ), namely  $\delta v_i^{(k)}$ , is calculated by subtracting the *material*<sub>1</sub> volume fractions between two of its successive unit cell configurations corresponding to the  $(k)^{th}$  and  $(k+1)^{th}$  element of its geometric parameter vector (see [Figure 4](#)). The homogenization of the mechanical properties has been performed on a  $[40 \times 40 \times 40]$  discretization mesh for all microstructure types by implementation of the MATLAB code in [Guoying et al. \(2018\)](#).

For computational saving purposes, the penalty factor  $p$  has been set equal to unity while the *material*<sub>1</sub> volume fraction equal to 0.3. The maximum number of iterations has been set equal to  $maxloop = 200$  and the prescribed tolerance to  $tolx = 10^{-4}$ , which is compared at the end of each optimization loop with the  $L_\infty$  norm of the change in the design vector between two successive iterations (see the pseudo-code listed in [Table A1](#)). No filters have been applied during the optimization process, as such the derivatives of all design functions are calculated with respect to the true design variables. Finally, it is reported that all optimization problems have been solved by means of the MMA solution algorithm, although gradient-free solution algorithms when coupling the objective function with the imposed

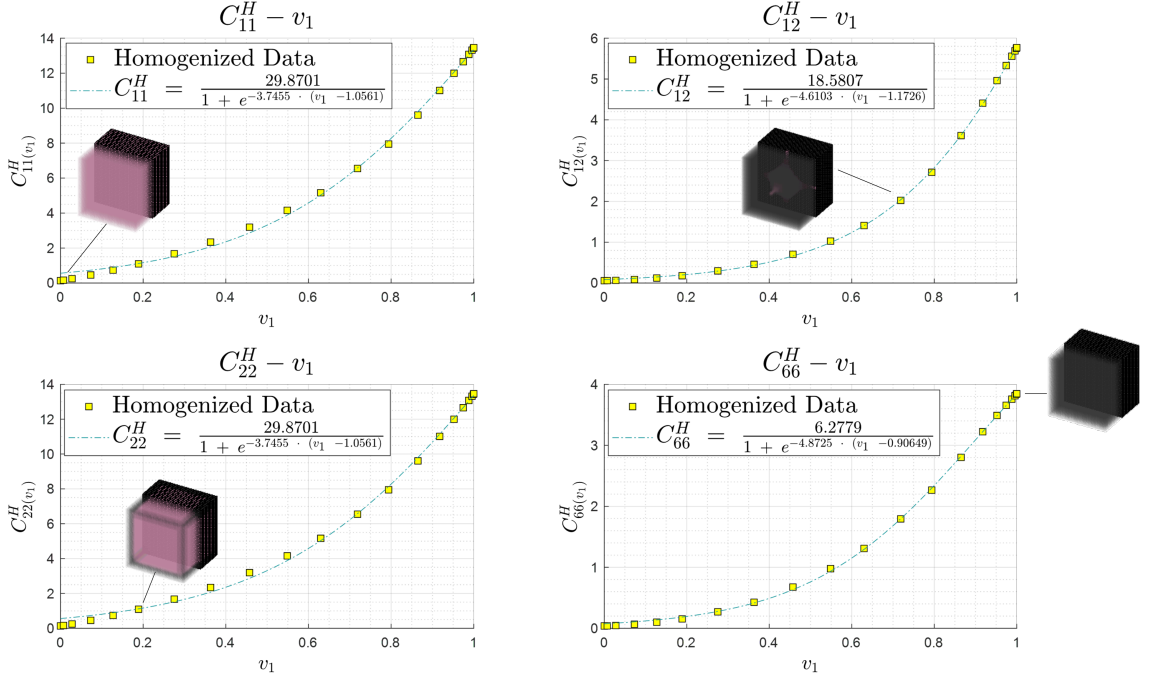


**Figure 10:** The three parameter *sigmoid* model is selected for fitting all terms of the homogenized elasticity tensor to the  $material_1$  volume fractions for all microstructure types. The regression process is depicted for the main terms of the 'Lattice' microstructure (due to the microstructure's cubic symmetry).

Table 4: The design parameters of the numerical examples

	<b>MBB Beam</b>
Discretization mesh	$[40 \times 40 \times 20]$
$material_1$ volume fraction	$f_{volfrac}^1 = 0.3$
Penalty factor	$p = 1$
Filter	-
Scale ratio	$\epsilon_i = 10^{-3}, \quad i = 1 : 3$
Maximum iterations number	$maxloop = 200$
$L_\infty$ tolerance	$tolx = 10^{-4}$
$material_1$ display threshold	0.4
Symmetry conditions	Not imposed

constraints, e.g., see the Augmented Lagrangian Method (ALM) (Vanderplaats (1984)), might perform better than the gradient-based ones.

### 6.1. Test example 1: Considering the 'Cylindrical' microstructure of two candidate fiber orientations for the MBB beam

In this test example, of the four microstructure types only the 'Cylindrical' one is examined; two candidate orientations are considered for the fiber: one with its axis being aligned with the  $x_2$  axis of the global coordinate

system and one forming a  $90^0$  angle with it, as shown in [Figure 11](#). In this case, the design variable vector of the  $(e)$  FE takes the form:  $\{dv\}_e = [\xi_e, v_{e1}, v_{e2}]$ , where  $\xi_e$  the natural coordinate of the 1D linear FE, and  $v_{e1}, v_{e2}$  the *material*<sub>1</sub> volume fractions corresponding the the ' $0^0$  rotated' and ' $90^0$  rotated' configurations, respectively. The corresponding SFP-based HTDMOP is posed as listed in the second column of [Table 3](#). Here, instead of implementing Eq.(5) to derive the shape functions of the 1D linear FE, their simplified expression listed in [Table 3](#) is preferred. As such, the  $\xi_e$  design variable is defined within the  $[0, 1]$  and not the  $[-1, 1]$  range. The bounds concerning the *material*<sub>1</sub> volume fraction within the '*Cylindrical*' microstructure are listed in [Table 2](#).

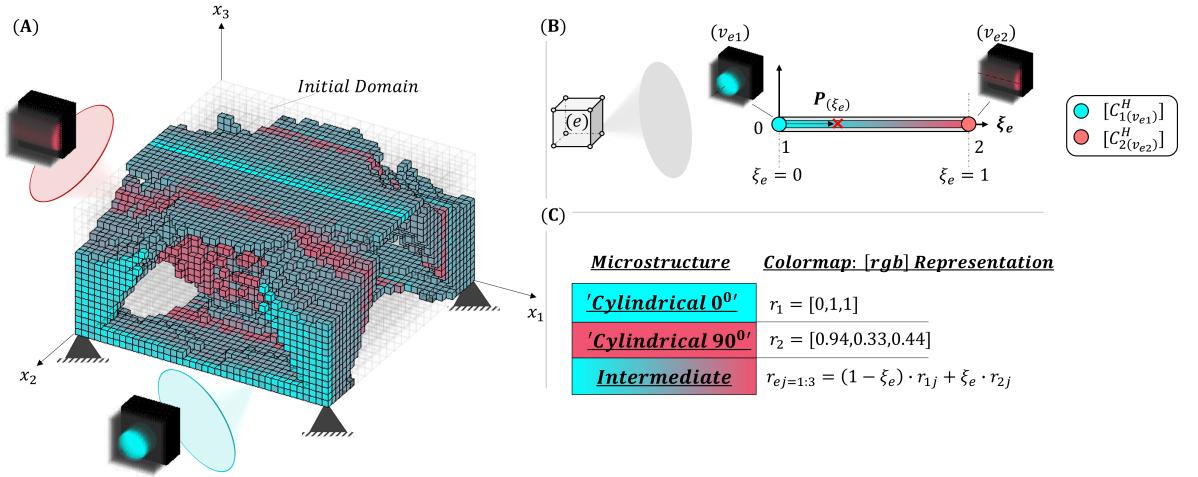


**Figure 11:** Test example 1: **(A)** The optimal microstructure type predicted for the MBB beam. **(B)** The shape functions of the 1D linear FE are employed to interpolate the candidate homogenized properties within the  $(e)$  element. **(C)** The SFP interpolation scheme is adopted for depicting the intermediate configurations.

The optimal microstructure type predicted for the MBB beam at the end of the 200<sup>th</sup> iteration is depicted in [Figure 11](#). The display threshold for the *material*<sub>1</sub> volume fraction has been set equal to 0.4 *i.e.*, only elements of *material*<sub>1</sub> volume fraction  $v_e \geq 0.4$  are displayed. The intermediate values predicted for the  $\xi_e$  design variables at the end of the optimization process, namely  $\xi_{e=1:N}^* \in (0, 1)$ , are visualized in the figure by adopting the SFP interpolation scheme for the [rgb] colors assigned to the candidate microstructures. In the present case, the  $\xi_e^*$  values do carry a physical meaning as they indicate that fiber angles within the  $(0^0, 90^0)$  range are more optimal than the ones initially considered. The metric quantifying the deviation of the continuous (or relaxed) solution from its nearest discrete (or feasible) value is defined as the *non-discreteness* of the final design. In this example, one way of reducing the degree of non-discreteness in the final design is to consider additional '*Cylindrical*' microstructures of intermediate fiber orientations as candidates for each element in the domain, the homogenized properties of which can be interpolated

within it via the deployment of a higher dimensional  $2^k$ -noded FE's shape functions, *i.e.*  $k \in \mathbb{N}_{\neq 1}^+$ . Alternative techniques for reducing the degree of non-discreteness in the final design are discussed in the next example.

## 6.2. Test example 2: Considering the {'Lattice', 'Box', 'Cylindrical', 'Spherical'} microstructures as candidates for the MBB beam

In this example, all four microstructure types are considered for the MBB beam. In this case, the  $\{dv\}_e$  design variable vector takes the form:  $\{dv\}_e = [\xi_{e1}, \xi_{e2}, v_{e1}, v_{e2}, v_{e3}, v_{e4}]$  where  $\{\xi_e\} = (\xi_{e1}, \xi_{e2})$  the natural coordinates of the 4-noded quadrangular FE and  $v_{ei}$  the *material*<sub>1</sub> volume fraction of the ( $i^{\text{th}}$ ) in order candidate microstructure. The respective SFP-based HTDMOP is listed in the last column of Table 3. With regard to the side constraints of the optimization problem, the  $\{\xi_e\}$  vector is defined within the  $[-1, 1]^2$  rectangle, while the bounds of the *material*<sub>1</sub> volume fraction for each microstructure are listed in Table 2. The optimal microstructure type predicted for the MBB beam at the end of the 200<sup>th</sup> optimization loop is depicted in Figure 12.

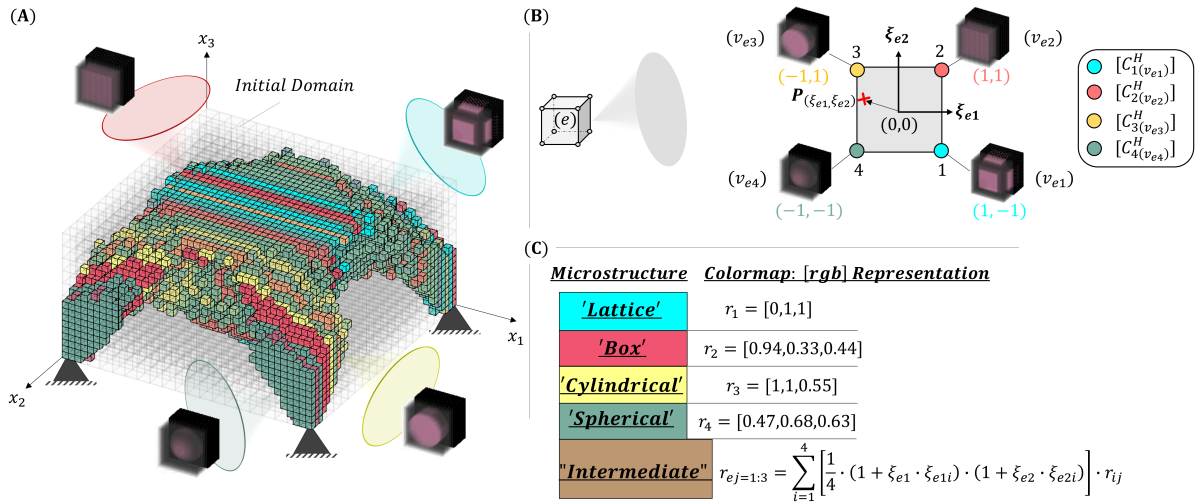


**Figure 12:** Test example 2: (A) The optimal microstructure type predicted for the MBB beam. (B) The shape functions of the 4-noded quadrangular FE are employed to interpolate the candidate homogenized properties within the ( $e$ ) element. (C) The SFP interpolation scheme is adopted for depicting the "intermediate" configurations.

Contrary to the previous test example, the predicted "intermediate" microstructure types do not carry any physical meaning, and it is becoming clear that a high degree of non-discreteness in the final design can quickly become a bottleneck for the microstructure type optimization problem. In this respect, three techniques are presented aiming to reduce the degree of non-discreteness in the final design, which can either be combined or applied separately:

**(1) Increasing the penalty factor  $p$ :** Greater values than that of the unity set for the penalty factor shift the intermediate values of the shape functions towards their  $\{0, 1\}$  bounds, leading thus to a "more discrete" solution. As

discussed in (Sec. 5.3), the computational intensiveness that comes with this approach is reflected in the high degree of non-convexity of the resulting SFP-based HTDMOP. Nonetheless, penalizing design variables that are discrete in nature but for computational purposes are treated as continuous, is the most popular approach for the majority of non-linear DP problems. As the effect of the penalty factor on the degree of discreteness in the final design is very well documented in the literature, from numerical techniques such as SIMP, DMO, SFP, *etc.*, it is not explored any further in this work. Moreover, with regard to the original utilization of the SFP technique in the framework of fiber orientation optimization for laminated composite structures, the authors have already demonstrated the effect of the penalty factor on the discreteness of the continuous solution (see Bruyneel (2011)).

**(2) Rounding the continuous solution to the nearest discrete design:** This process operates as the post-processing stage of the whole analysis, where the design predicted after solving the SFP-based HTDMOP is rounded to the nearest feasible one. It is important to point out that the rounding process takes place only for the  $\{\Xi\}^* = \bigcup_{e=1}^N \{\xi_e\}^*$  design variables, as they are the only ones defined within a discrete set, namely the set formed by the nodal coordinates of the  $2^k$ -noded quadrangular FE (the *material*<sub>1</sub> volume fractions are continuous design variables). For instance, in the present case where four candidate microstructures are considered per element in the domain, this approach implies rounding the  $\{\xi_e\}^*$  continuous solutions to the nearest nodal coordinate of the 4-noded quadrangular FE, *i.e.* the following process take place:  $\{\xi_e\}^* \rightarrow \{\xi_e\}^{d*} \in \{(1, -1), (1, 1), (-1, 1), (-1, -1)\}$ , with  $(e) = 1 : N$ .

Generalizing the rounding process for the case of  $2^k$  candidate microstructures translates into rounding the  $\{\xi_e\}^*$  solutions to the nearest vertex coordinate of the  $[-1, 1]^k$  hyper-rectangle. However, rounding the continuous solutions to the nearest feasible one rises potential issues, such as leading to infeasible design points, where some of the design constraints may be violated or even lead to feasible designs significantly worse than the best discrete design. Figure 13 illustrates the effect that rounding the continuous solution  $\{\Xi\}^* = \bigcup_{e=1}^N \{\xi_e\}^*$  to the nearest discrete one  $\{\Xi\}^{d*} = \bigcup_{e=1}^N \{\xi_e\}^{d*}$  bears on the volume constraint imposed on the *material*<sub>1</sub> component for the current test example. As shown in the figure, rounding the continuous solution resulted in a 9.52% reduction in the final value of the volume constraint. This violation is a direct consequence of the constraint's dependence on the  $\{\xi_e\}$  design variables as stated in Eq.(13).

**(3) Imposing the degree of non-discreteness as an additional constraint on the SFP-based HTDMOP:** The idea of introducing a metric to quantify the non-discreteness in the design is discussed in (Sigmund (2007), Sørensen et al. (2014)). Similarly, a metric is developed in this work as to quantify the non-discreteness in the final design. Establishing that the non-discreteness in the design originates solely from the  $\{\xi_e\}$  design variables, implies that the developed

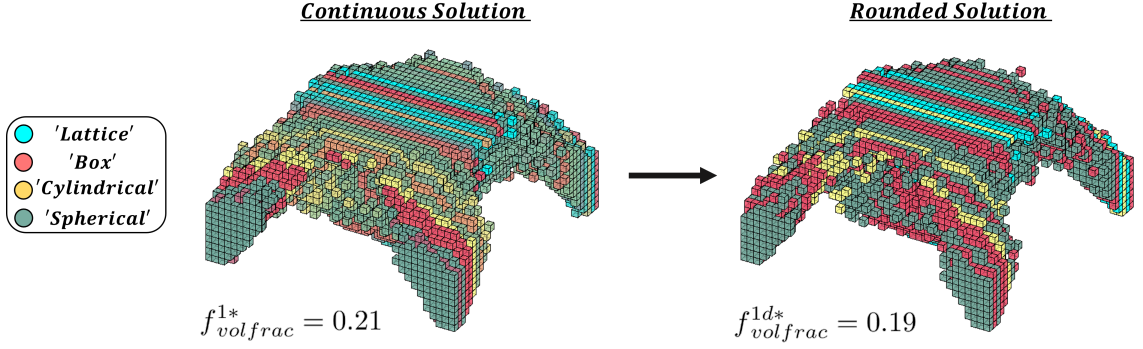


**Figure 13:** Rounding the continuous solution to the nearest discrete one may result in violation of the final value of the design functions.

metric should be a function of them alone. Further, it should predict a 0% non-discreteness in the continuous solution at the nodal coordinates of the  $2^k$ -quadrangular FE, where the discrete designs (*i.e.* the candidate microstructures) are allocated, and a 100% non-discreteness at its center, where no discrete designs are assigned. In this respect, the authors propose the following metric that meets the above conditions:

$$m_{end(\{\xi_e\})} = \prod_{i=1}^{2^k} \left( \frac{1 - N^p \cdot ei(\{\xi_e\})}{1 - \frac{1}{2^{k \cdot p}}} \right) \cdot 100\% \quad \text{with } e = 1 : N. \quad (19)$$

As a reminder, in Eq.(19)  $p$  is the penalty factor,  $k$  is the dimension of the hyper-rectangle the  $\{\xi_e\}$  variables are defined within, and  $N$  the number of FEs discretizing the structural domain. Calculated at any node of the quadrangular FE, the above metric returns a 0% non-discreteness in the continuous solution, while calculated at the center of the quadrangular FE returns a 100% non-discreteness in the solution. The last property holds due to the fact that all shape functions equal to  $\frac{1}{2^{k \cdot p}}$  at the center of the element, and as a result all fractions in the product are divided out (are equal to unity). For computational purposes, the  $N$ -dimensional vector of metrics is collapsed into a global, scalar-valued metric concerning the entire domain as follows:

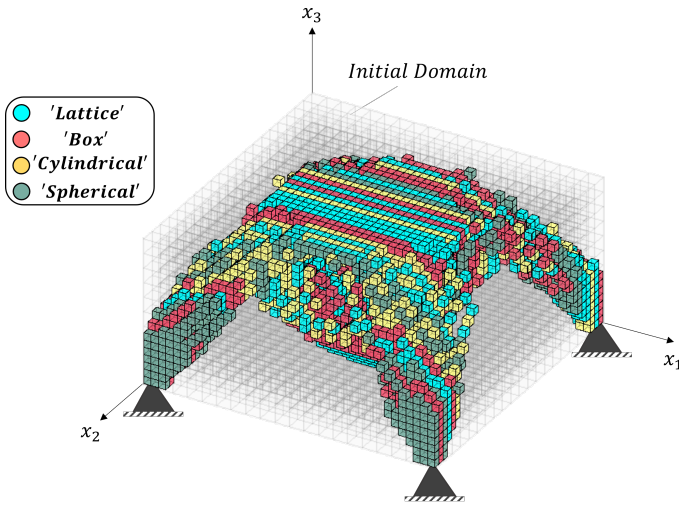
$$M_{gnd(\{\Xi\})} = \frac{1}{N} \cdot \left( \sum_{e=1}^N (m_{end})^2 \right) = \frac{1}{N} \cdot \left( \sum_{e=1}^N \prod_{i=1}^{2^k} \left( \frac{1 - N^p \cdot ei(\{\xi_e\})}{1 - \frac{1}{2^{k \cdot p}}} \right)^2 \right) \cdot 100\%, \quad (20)$$

where  $\{\Xi\} = \bigcup_{e=1}^N \{\xi_e\} \in [-1, 1]^{N \cdot k}$ . Finally, the constraint concerning the permissible degree of global non-discreteness in the design is expressed as follows:

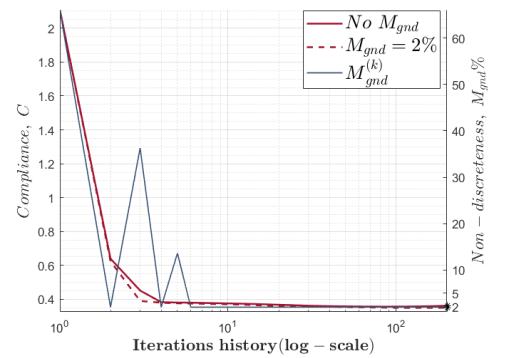
$$M_{G(\{\Xi\})} : M_{gnd(\{\Xi\})} - M_{all} = 0, \quad (21)$$

where  $M_{all}$ , the imposed percentage of global non-discreteness in the design (the above constraint could as well be posed as an in-equality constraint, as to allow the search of the solution in a larger design space).

In this example,  $k = 2$ ,  $p = 1$ , and the number of FEs in the domain are  $N = 32 \cdot 10^3$ . Repeating test example 2 but now with the constraint of  $M_{all} = 2\%$  in the global non-discreteness of the final design added to the initial optimization problem, the new microstructure type distribution predicted for the MBB beam is as depicted in Figure 14<sub>a</sub>. For comparison, Figure 15 illustrates the distribution of the metric stated in Eq.(19) in the final designs corresponding to the case where the 2% constraint in the global non-discreteness has been omitted and included in the SFP-based HTDMOP, respectively.



(a) The optimal microstructure type predicted for the MBB beam.



(b) The convergence history of the compliance when omitting and when including the constraint of the global non-discreteness in the SFP-based HTDMOP (in red continuous and dashed line, respectively). For the latter case, the convergence history of the global metric  $M_{gnd}$  is displayed along. The graph is given in semi-logarithmic scale.

**Figure 14:** Test example 2 with the addition of the 2% constraint in the global non-discreteness.

## 7. Extensions of the methodology

The following modifications can be applied to the proposed methodology:

**(1) Considering more complex microstructures:** The methodology has been built upon simplified (uni-variate) microstructures, where a single geometric parameter explicitly defines the configuration of the unit cell, *i.e.*, there has been assumed a one-to-one correspondence between configuration and geometric parameter of the unit cell. However, more complex microstructures of more than one geometric parameters can be considered instead, at the unavoidable computational expense that comes with adding more design variables to the SFP-based HTDMOP. In this case, contrary to the microstructures considered for this work, the monotonicity of the  $material_1$  volume fraction with the geometric parameters of the unit cell is not guaranteed, since different combinations of their geometric parameters may result to

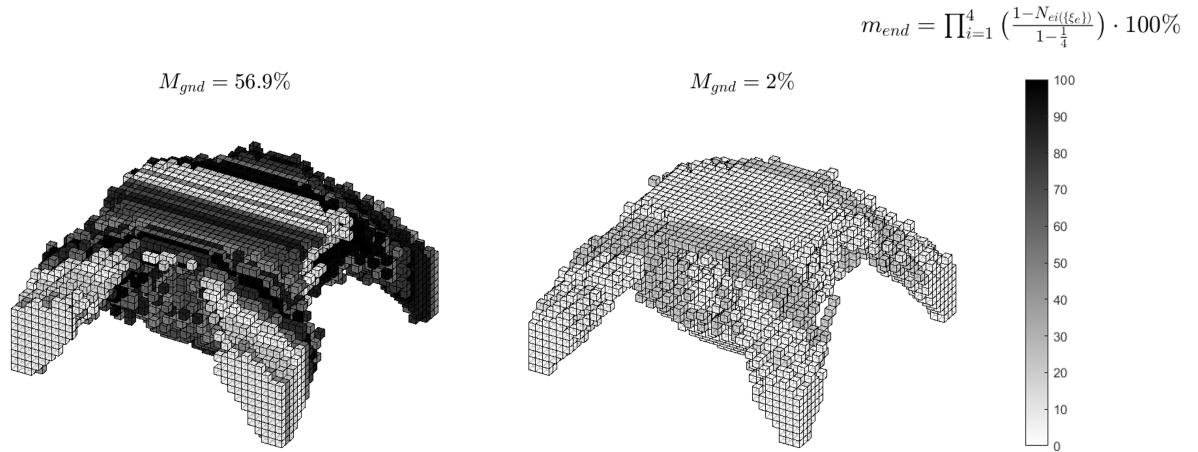


**Figure 15:** Distribution of the non-discreteness metric in the final designs: **Left-hand side:** Without imposing a constraint in the global non-discreteness. **Right-hand side:** When imposing a 2% constraint in the global non-discreteness.

the same  $material_1$  volume fraction. Therefore, it is essential to first establish the monotonicity between the  $material_1$  volume fraction and the geometric parameters of the unit cell, and then determine which of the two is more efficient to serve as the design variable in the SFP-based HTDMOP.

**(2) Working in patches:** In the numerical examples demonstrated a unique microstructure has been assumed for each element in the structural domain; assigning a group of elements the same candidate microstructures, the methodology can operate on the level of the so-called 'patches' rather than on individual elements. The  $\{\xi_e\}$  design variable vector that was initially tied to each individual element ( $e$ ), is now tied to each patch  $l$  of the structural domain, *i.e.* the following replacement takes place in the notation:  $\{\xi_e\} \rightarrow \{\xi_l\} \in [-1, 1]^{k_l} \forall l = 1 : L$  where,  $L$  is the number of patches the domain is divided into, and each patch  $l$  is assigned  $2^{k_l}$  candidate microstructures, where  $k_l \in \mathbb{N}^+$ .

**(3) Concurrent homogenization-based topology, multi-material and/or microstructure type optimization:** As depicted in Figures 7<sub>B</sub> & 8, the methodology can be tailored into the concurrent homogenization-based topology, multi-material and microstructure type optimization problem, provided that the material the volume constraint is imposed on constitutes one of the two components for all candidate microstructures. Employing the shape functions of higher dimension FEs, different candidate microstructure types of the same material components and/or the same microstructure types of different  $material_2$  components can be allocated to its nodes.

**(4) Deploying a different material interpolation technique:** The methodology has been formulated based on the assumption that the SFP technique is employed to interpolate the candidate homogenized properties within the structural domain. However, in the framework of discrete material optimization, there is a variety of interpolation techniques proposed in the literature to select from. To the ones listed in the introduction, the more recent works of Kiyono et al. (2016), Ypsilantis et al. (2022) are appended.

## 8. Replication of results

The pseudo-code for solving the SFP-based HTDMOP posed in (Sec. 5.3) is listed in Table A1. The authors recommend incorporating random restarts ( *i.e.* initial design points) when using gradient-based solution algorithms, since the returned solution is very likely to be trapped in a local minimum. Further, it is underscored that the SFP-based HTDMOP is not tied to a specific solution algorithm, as such different solution algorithms can be implemented for solving it.

## 9. Concluding remarks

This work proposes a methodology for the concurrent optimization of the type and configuration of the microstructure of the structural domain from a catalogue of pre-defined candidate microstructures. To this end, the DMOP is combined with the HTOP for compliance minimization of the structure. The methodology is gradually built up through the example where four candidate microstructure types of the same two distinct material components are considered for the structural domain. Based on these auxiliary microstructures the SFP-based HTDMOP is formulated and generalized for the case of  $2^k$  candidate microstructures, where  $k \in \mathbb{N}^+$ . Further, it is demonstrated that the mathematical framework derived for the SFP-based HTDMOP can be implemented as is in different classes of optimization problems, such as the concurrent homogenization-based topology, multi-material and/or microstructure type optimization of the structure.

## 10. Acknowledgements

- "Konstantinos-Iason Ypsilantis acknowledges the support of the Research Foundation Flanders (FWO) under the grant number 1SA8721N"

## References

- Alexandersen, J., & Lazarov, B. (2015). Topology optimization of manufacturable microstructural details without length scale separation using a spectral coarse basis preconditioner. *Computer Methods in Applied Mechanics and Engineering*, 290, 156–182. URL: <https://doi.org/10.1016/j.cma.2015.02.028>. doi:10.1016/j.cma.2015.02.028.
- Allaire, G. (2002). *Shape Optimization by the Homogenization Method*, Applied Mathematical Sciences volume 146 of Applied Mathematical Sciences. Springer. doi:10.1007/978-1-4684-9286-6.
- Allaire, G., Geoffroy-Donders, P., & Pantz, O. (2019). Topology optimization of modulated and oriented periodic microstructures by the homogenization method. *Computers Mathematics with Applications*, 78, 2197–2229. URL: <https://doi.org/10.1016/j.camwa.2018.08.007>. doi:10.1016/j.camwa.2018.08.007.

- Andreassen, E., & Andreassen, C. S. (2014). How to determine composite material properties using numerical homogenization. *Computational Materials Science*, 83, 488–495. URL: <https://doi.org/10.1016/j.commatsci.2013.09.006>. doi:10.1016/j.commatsci.2013.09.006.
- Andreassen, E., Clausen, A., Schevenels, M., Lazarov, B. S., & Sigmund, O. (2011). Efficient topology optimization in matlab using 88 lines of code. *Structural Multidisciplinary Optimization*, 43, 1–16. URL: <https://doi.org/10.1007/s00158-010-0594-7>. doi:10.1007/s00158-010-0594-7.
- Bendsøe, M. P. (1989). Optimal shape design as a material distribution problem. *Structural and Multidisciplinary Optimization*, 1, 193–202. URL: <https://doi.org/10.1007/BF01650949>. doi:10.1007/BF01650949.
- Bendsøe, M. P., & Kikuchi, N. (1988). Generating optimal topologies in structural design using a homogenization method. *Computer Methods in Applied Mechanics and Engineering*, 71, 197–224. URL: [https://doi.org/10.1016/0045-7825\(88\)90086-2](https://doi.org/10.1016/0045-7825(88)90086-2). doi:10.1016/0045-7825(88)90086-2.
- Bendsøe, M. P., & Sigmund, O. (2004). *Topology optimization: Theory, Methods and Applications*. (2nd ed.). Berlin Heidelberg: Springer-Verlag. doi:10.1007/978-3-662-05086-6.
- Bensoussan, A., Lions, J. L., & Papanicolaou, G. (1978). *Asymptotic analysis for periodic structures* volume 7. (1st ed.). New York: North Holland.
- Bruyneel, M. (2011). SFP– a new parameterization based on shape functions for optimal material selection: application to conventional composite plies. *Structural and Multidisciplinary Optimization*, 43, 17–27.
- Bruyneel, M., Duysinx, P., Fleury, C., & Gao, T. (2011). SFP: Extensions of the shape functions with penalization (sfp) parameterization for composite plies optimization. *American Institute of Aeronautics and Astronautics*, 49, 979–1006. URL: <https://doi.org/10.2514/1.J051225>. doi:10.2514/1.J051225.
- Chen, W., Tong, L., & Liu, S. (2017). Concurrent topology design of structure and material using a two-scale topology optimization. *Computer & Structures*, 178, 119–128. URL: <https://doi.org/10.1016/j.compstruc.2016.10.013>. doi:10.1016/j.compstruc.2016.10.013.
- Christensen, P. W., & Klarbring, A. (2009). *An introduction to Structural Optimization* volume 153 of *Solid Mechanics and Its Applications*. Netherlands: Springer. doi:10.1007/978-1-4020-8666-3.
- Da, D., Cui, X., Long, K., & Li, G. (2017). Concurrent topological design of composite structures and the underlying multi-phase materials. *Computer & Structures*, 179, 1–148. URL: <https://doi.org/10.1016/j.compstruc.2016.10.006>. doi:doi.org/10.1016/j.compstruc.2016.10.006.
- Ferrari, F., & Sigmund, O. (2020). A new generation 99 line matlab code for compliance topology optimization and its extension to 3d. *Structural and Multidisciplinary Optimization*, 62, 2211–2228. URL: <https://doi.org/10.1007/s00158-020-02629-w>. doi:10.1007/s00158-020-02629-w.
- Fujii, D., Chen, B. C., & Kikuchi, N. (2001). Composite material design of two-dimensional structures using the homogenization design method. *International Journal for Numerical Methods in Engineering*, 50, 2031–2051. URL: <https://doi.org/10.1002/nme.105>. doi:10.1002/nme.105.
- Gao, J., Zhen, L., Liang, X., & Liang, G. (2019). Concurrent topology optimization of multiscale composite structures in matlab. *Structural and Multidisciplinary Optimization*, 60, 2621–2651. URL: <https://doi.org/10.1007/s00158-019-02323-6>. doi:10.1007/s00158-019-02323-6.
- Gao, T., Zhang, W., & Duysinx, P. (2012). A bi-value coding parameterization scheme for the discrete optimal orientation design of the composite laminate. *International Journal for Numerical Methods in Engineering*, 91, 98–114. URL: <https://onlinelibrary.wiley.com/doi/abs/10.1002/nme.4270>. doi:<https://doi.org/10.1002/nme.4270>.

- Groen, J., Stutz, F., Aage, N., Bærentzen, J., & Sigmund, O. (2020). De-homogenization of optimal multi-scale 3d topologies. *Computer Methods in Applied Mechanics and Engineering*, 364. URL: <https://doi.org/10.1016/j.cma.2020.112979>. doi:10.1016/j.cma.2020.112979.
- Guoying, D., Yunlong, T., & Yaoyao, F. Z. (2018). A 149 line homogenization code for three-dimensional cellular materials written in matlab. *Journal of Engineering Materials and Technology*, 141, 488–495. URL: <https://doi.org/10.1115/1.4040555>. doi:10.1115/1.4040555.
- Hassani, B., & Hinton, E. (1998a). A review of homogenization and topology optimization II analytical and numerical solution of homogenization equations. *Computers and Structures*, 69, 719–738. URL: [https://doi.org/10.1016/S0045-7949\(98\)00132-1](https://doi.org/10.1016/S0045-7949(98)00132-1). doi:10.1016/S0045-7949(98)00132-1.
- Hassani, B., & Hinton, E. (1998b). A review of homogenization and topology optimization III -topology optimization using optimality criteria. *Computers and Structures*, 69, 739–756. URL: [https://doi.org/10.1016/S0045-7949\(98\)00133-3](https://doi.org/10.1016/S0045-7949(98)00133-3). doi:10.1016/S0045-7949(98)00133-3.
- Hassani, B., & Hinton, E. (1998c). A review of homogenization and topology optimization I—homogenization theory for media with periodic structure. *Computers and Structures*, 69, 707–717. URL: [https://doi.org/10.1016/S0045-7949\(98\)00131-X](https://doi.org/10.1016/S0045-7949(98)00131-X). doi:10.1016/S0045-7949(98)00131-X.
- Kiyono, C. Y., Silva, E. C. N., & Reddy, J. N. (2016). A novel fiber optimization method based on normal distribution function with continuously varying fiber path. *Composite Structures*, 160, 503–515. doi:10.1016/j.compstruct.2016.10.064.
- Kumar, T., & Suresh, K. (2021). Direct lagrange multiplier updates in topology optimization. *Structural and Multidisciplinary Optimization*, 63, 1563–1578. URL: <https://doi.org/10.1007/s00158-020-02740-y>. doi:10.1007/s00158-020-02740-y.
- Lazarov, B. (2013). Topology optimization using multiscale finite element method for high-contrast media. In *International Conference on Large-Scale Scientific Computing-LSSC 2013*. Sozopol, Bulgaria.
- Li, H., Luo, Z., Gao, L., & Qin, Q. (2018). Topology optimization for concurrent design of structures with multi-patch microstructures by level sets. *Computer Methods in Applied Mechanics and Engineering*, 331, 536–561. URL: <https://doi.org/10.1016/j.cma.2017.11.033>. doi:10.1016/j.cma.2017.11.033.
- Liu, K., & Tovar, A. (2014). An efficient 3d topology optimization code written in matlab. *Structural Multidisciplinary Optimization*, 50, 1175–1196. URL: <https://doi.org/10.1007/s00158-014-1107-x>. doi:10.1007/s00158-014-1107-x.
- Liu, L., Yan, J., & Cheng, G. (2008). Optimum structure with homogeneous optimum truss-like material. *Computers and Structures*, 86, 1417–1425. URL: <https://doi.org/10.1016/j.compstruc.2007.04.030>. doi:10.1016/j.compstruc.2007.04.030.
- Monteiro, A. (2017). *Topology Optimization of Microstructures with Constraints on Average Stress and Material Properties*. Master's thesis Instituto Superior Técnico, Universidade de Lisboa Portugal.
- Pantz, O., & Trabelsi, K. (2008). A post-treatment of the homogenization method for shape optimization. *SIAM Journal on Control and Optimization*, 47, 1380–1398. URL: <https://doi.org/10.1137/070688900>. doi:10.1137/070688900.
- Pantz, O., & Trabelsi, K. (2010). Construction of minimization sequences for shape optimization. In *15th International Conference on Methods and Models in Automation and Robotics* (pp. 278–283). Miedzyzdroje, Poland. URL: <https://doi.org/10.1109/MMAR.2010.5587222>. doi:10.1109/MMAR.2010.5587222.
- Pizzolato, A., Sharma, , Maute, , Sciacovelli, A., & Verda, V. (2019). Multi-scale topology optimization of multi-material structures with controllable geometric complexity— applications to heat transfer problems. *Comput. Methods Appl. Mech. Engrg.*, 357, 112552. doi:doi.org/10.1016/j.cma.2019.07.02.
- Rana, S., & Fangueiro, R. (2006). *Advanced Composite Materials for Aerospace Engineering*. Woodhead Publishing (1st ed.). Elsevier.

- Rodrigues, H., Guedes, J., & Bendsøe, M. P. (2002). Hierarchical optimization of material and structure. *Structural and Multidisciplinary Optimization*, 24, 1–10. URL: <https://doi.org/10.1007/s00158-002-0209-z>. doi:10.1007/s00158-002-0209-z.
- Rozvany, G. I. N., & Olhoff, N. (2001). *Topology Optimization of Structures and Composite Continua* volume 7 of *Nato Science Series II*. (1st ed.). Netherlands: Springer.
- Sigmund, O. (2001). A 99 line topology optimization code written in matlab. *Structural Multidisciplinary Optimization*, 21, 120–127. URL: <https://doi.org/10.1007/s001580050176>. doi:10.1007/s001580050176.
- Sigmund, O. (2007). Morphology-based black and white filters for topology optimization. *Structural and Multidisciplinary Optimization*, 33, 401–424. URL: <https://link.springer.com/article/10.1007/s00158-006-0087-x>. doi:10.1007/s00158-006-0087-x.
- Sørensen, S. N., Sørensen, R., & Lund, E. (2014). Dmto - a method for discrete material and thickness optimization of laminated composite structures. *Structural and Multidisciplinary Optimization*, 50, 25–47. URL: <https://link.springer.com/article/10.1007/s00158-014-1047-5>. doi:10.1007/s00158-014-1047-5.
- Stegmann, J. (2004). *Analysis and optimization of laminated composite structures*. Ph.D. thesis Aalborg University.
- Stegmann, J., & Lund, E. (2005). Discrete material optimization of general composite shell structures. *International Journal for Numerical Methods in Engineering*, 62, 2009–2027. URL: <https://doi.org/10.1002/nme.1259>. doi:10.1002/nme.1259.
- Svanberg, K. (1987). The method of moving asymptotes - a new method for structural optimization. *International Journal for Numerical Methods in Engineering*, 24, 359–373. URL: <https://doi.org/10.1002/nme.1620240207>. doi:10.1002/nme.1620240207.
- Vanderplaats, G. N. (1984). *Numerical Optimization Techniques for Engineering Design: with Applications*. New York: McGraw-Hill.
- Wang, Y., Luo, Z., Kang, Z., & Zhang, N. (2015). A multi-material level set-based topology and shape optimization method. *Comput. Methods Appl. Mech. Engrg.*, 283, 1570–1586. doi:10.1016/j.cma.2014.11.002.
- Wang, Y., Wang, M. Y., & Chen, F. (2016). Structure-material integrated design by level sets. *Structural and Multidisciplinary Optimization*, 54, 1145–1156. URL: <https://doi.org/10.1007/s00158-016-1430-5>. doi:10.1007/s00158-016-1430-5.
- Wrenn, G. (1989). *An Indirect Method for Numerical Optimization Using the Kreisselmeier-Steinhauser Function*. NASA Contractor Report. URL: <https://ntrs.nasa.gov/citations/19890007408>.
- Wu, J., Wang, W., & Gao, X. (2019). Design and optimization of conforming lattice structures. *IEEE Transactions on Visualization and Computer Graphics*, . URL: <https://doi.org/10.1109/TVCG.2019.2938946>. doi:10.1109/TVCG.2019.2938946.
- Xia, L., Xia, Q., Huang, X., & Xie, Y. (2018). Bi-directional evolutionary structural optimization on advanced structures and materials: A comprehensive review. *Archives of Computational Methods in Engineering*, 25, 437–478. doi:10.1007/s11831-016-9203-2.
- Yan, X., Huang, X., Zha, Y., & Xie, Y. (2014). Concurrent topology optimization of structures and their composite microstructures. *Computer & Structures*, 133, 103–110. URL: <http://dx.doi.org/10.1016/j.compstruc.2013.12.001>. doi:10.1016/j.compstruc.2013.12.001.
- Ypsilantis, K. I., Faes, M., Ivens, J., & Moens, D. (2022). A material interpolation technique based on the simplex polytope. In *8th European Congress on Computational Methods in Applied Sciences and Engineering*. Oslo, Norway.
- Zhou, M., & Rozvany, G. I. N. (1991). The COC algorithm, part ii: Topological, geometrical and generalized shape optimization. *Computer Methods in Applied Mechanics and Engineering*, 89, 309–336. URL: [https://doi.org/10.1016/0045-7825\(91\)90046-9](https://doi.org/10.1016/0045-7825(91)90046-9). doi:10.1016/0045-7825(91)90046-9.

Table A1: Pseudo-code for solving the SFP-based HTDMOP (Case of  $2^K$  candidate microstructures,  $K \in \mathbb{N}^+$ )

---

```

%% Initialization of the design variables
% Design variable vector of the (e) element:
 $\{dv\}_e^{(1)} = [-1 + 2 \cdot rand(1, K), \max(f_{volfrac}^1, [v_{1,min}, \dots, v_{2^K,min}])]; \quad \forall e = 1 : N$ 
% Global Design Variable Vector
 $\{dv\}^{(1)} = [\{dv\}_1^{(1)}, \dots, \{dv\}_e^{(1)}, \dots, \{dv\}_N^{(1)}]; \quad \%N \text{ the number of elements in the domain}$ 
%% Start the Optimization Loop
 $k = 1; \quad tol^{(1)} = 1 \quad \% \text{ the lowercase } k \text{ stands for the iteration number}$ 
while ( $k \leq \text{maxloop} \parallel tol^{(k)} \geq \text{tolx}$ )
%% FEA
Calculate the element's stiffness matrix:  $[K_{e(\{dv\}_e^{(k)})}]$ ,  $e = 1 : N \quad \dots(\text{Eq.}(8))$ 
Calculate the global stiffness matrix:  $[K_{all}]^{(k)} = \sum_{e=1}^N [K_{e(\{dv\}_e^{(k)})}]$ 
Calculate the global displacement vector:  $\{U_{all}\}^{(k)} \quad \dots(\text{Eq.}(12))$ 
%% Calculate the Design Functions at the Current Iteration
Calculate the objective function:  $C^{(k)} \quad \dots(\text{Eq.}(11))$ 
Calculate the volume constraint:  $F^{(k)} \quad \dots(\text{Eq.}(13))$ 
Calculate the shape functions summation constraint set (if  $p \neq 1$ ):  $h_e^{*(k)} \quad e = 1 : N \quad \dots(\text{Eq.}(18))$ 
%% Perform Sensitivity Analysis on the Design Functions
 $\left(\frac{dC}{\{dv\}_e}\right)^{(k)} = \begin{cases} \left(\frac{dC}{d\xi_{ej}}\right)^{(k)} = -\{U_{e(\{dv\}_e^{(k)})}\}^T \cdot \left(\frac{d[K_e]}{d\xi_{ej}}\right)^{(k)} \cdot \{U_{e(\{dv\}_e^{(k)})}\}, & j = 1 : K \quad \dots(\text{Eq.}(9)) \\ \left(\frac{dC}{dv_{ei}}\right)^{(k)} = -\{U_{e(\{dv\}_e^{(k)})}\}^T \cdot \left(\frac{d[K_e]}{dv_{ei}}\right)^{(k)} \cdot \{U_{e(\{dv\}_e^{(k)})}\}, & i = 1 : 2^K \quad \dots(\text{Eq.}(10)) \end{cases} \quad e = 1 : N$ 
 $\left(\frac{dF}{\{dv\}_e}\right)^{(k)} = \begin{cases} \left(\frac{dF}{d\xi_{ej}}\right)^{(k)} = \frac{\sum_{i=1}^{2^K} \left(\frac{dN_{ei}^p(\xi_e)}{d\xi_{ej}}\right)^{(k)} \cdot v_{ei}^{(k)}}{N \cdot f_{volfrac}^1}, & j = 1 : K \\ \left(\frac{dF}{dv_{ei}}\right)^{(k)} = \frac{(N_{ei}^p(\xi_e))^{(k)}}{N \cdot f_{volfrac}^1}, & i = 1 : 2^K \end{cases} \quad e = 1 : N$ 
 $\left(\frac{dh_e^*}{\{dv\}_e}\right)^{(k)} = \begin{cases} \left(\frac{dh_e^*}{d\xi_{ej}}\right)^{(k)} = (p \neq 1) \cdot \left(\sum_{i=1}^{2^K} \left(\frac{dN_{ei}^p(\xi_e)}{d\xi_{ej}}\right)^{(k)}\right), & j = 1 : K \\ \left(\frac{dh_e^*}{dv_{ei}}\right)^{(k)} = 0, & i = 1 : 2^K \end{cases} \quad e = 1 : N$ 
%% Call the Gradient-based Solution Algorithm
Obtain the next design point:  $\{dv\}^{(k+1)}$ 
%% Check Stopping Criteria
 $tol^{(k+1)} = \|\{dv\}^{(k+1)} - \{dv\}^{(k)}\|_\infty \quad \% \text{ Check the Inf norm between two successive iterations}$ 
if ( $\text{tolx} < tol^{(k)}$ )
 $\{dv\}^{(k+1)} = \{dv\}^{(k)}; \quad k = k + 1;$ 
else
break loop;
end
end
%% Obtain the Continuous Solution
 $\{dv\}^* = [\{dv\}_1^*, \dots, \{dv\}_e^*, \dots, \{dv\}_N^*]$  where,  $\{dv\}_e^* = [\xi_{e1}^*, \dots, \xi_{eK}^*; v_{e1}^*, \dots, v_{e2^K}^*]$ 

```

---